Results in Engineering 28 (2025) 107760

Contents lists available at ScienceDirect

Results in Engineering

journal homepage: www.sciencedirect.com/journal/results-in-engineering

Enhancement in fracture toughness and tribological stability of epoxy facilitated by heterogeneous 0D-0D nanofiller networks: An experimental and analytical evaluation

Gopal Krishna Bhagavatula [a], Snaha Leena [a], Rasana Nanoth [a,*], Alessandro Pegoretti [b], Jayanarayanan Karingamanna [a,*]

[a] Department of Chemical Engineering and Materials Science, Amrita School of Engineering, Coimbatore, Amrita Vishwa Vidyapeetham, 641112, India
[b] Department of Industrial Engineering, University of Trento, Via Sommarive 9, 38123 Trento, Italy

ARTICLE INFO

Keywords:
Fracture toughness
Tribological properties
Huang-kinloch toughness
Fleischer energy-based models

ABSTRACT

This work explores high-performance epoxy (EP) nanocomposites reinforced with silicon nitride (SiN) and tungsten carbide (WC) 0D-0D nanoparticles to overcome the intrinsic brittleness and weak wear resistance of EP. Both single-filler and dual-filler systems were developed and evaluated for their mechanical, fracture, and tribological behaviour. Among hybrid nanocomposites, ESW2 (0.25wt% SiN and 0.5wt% WC) exhibited the best overall performance, showing a remarkable increase in tensile strength, elastic modulus and strain by 130 %, 248 %, and 74 %, respectively, over EP. These improvements are attributed to SiN-induced crosslinking within the matrix and WC's anchoring and nanopolishing effects, offering a unique combination of stiffness, strength, and ductility. Tribological tests demonstrated that WC-filled and hybrid nanocomposites achieved a sharp reduction in wear rate and maintained stable COF under high loads, attributed to various wear mechanisms. Analysis of fracture behaviour revealed that Irwin's Linear Elastic Fracture Mechanics and the Huang-Kinloch models adequately described toughening in SiN-based systems through mechanisms such as plastic void growth and energy dissipation. However, WC-filled composites and hybrid nanocomposites exceeded theoretical predictions, revealing synergism. Wear and friction modelling further showed a reduction in frictional energy at higher loads, particularly for WC-based samples. Fleisher's model, surface roughness, and 3D surface plots confirmed WC's role in nanopolishing and transfer film formation, while SiN imparted thermal stabilization and micro-cutting resistance. In essence, this dual-filler epoxy system demonstrates a synergy by coupling toughness and wear resistance, making it ideal for engineering applications where mechanical integrity and abrasion resistance are demanded.

1. Introduction

Polymer nanocomposites consist of a continuous polymer phase and a dispersed nanofiller reinforcement phase. They provide the combined benefits of a polymer matrix (flexibility, processability, etc.) and the enhancement effects of nanofillers [1]. Nanocomposites exhibit superior performance over conventional composites, offering enhanced thermal and mechanical stability, improved efficiency, and increased stiffness [2]. Epoxy (EP), a class of thermosetting polymer, is widely used in automotive, aerospace, packaging, marine and adhesive applications, known for their appreciable strength and stiffness, chemical resistance, dimensional stability, thermal stability and low cost [3–6]. The major limitation of EP is its low toughness and brittle nature due to its cross-linking structure developed during the curing process [7]. The complex 3D structure of EP formed during curing results in a high coefficient of friction (COF) and low wear resistance [8]. Hence, the EP matrix is reinforced with nanofillers of various geometries to improve the toughness and wear resistance.

Polymer tribology deals with wear, frictional and lubrication behaviour of polymers in contact or relative motion against a counter-face. Among these three areas, wear and friction are commonly studied in polymeric materials and their composites. Polymer wear is a gradual material loss from the specimen's surface when sliding or rubbing against a counterface. They are analyzed under two sliding conditions

* Corresponding authors.
E-mail addresses: n_rasana@cb.amrita.edu (R. Nanoth), kj_narayanan@cb.amrita.edu (J. Karingamanna).

https://doi.org/10.1016/j.rineng.2025.107760
Received 29 June 2025; Received in revised form 11 September 2025; Accepted 15 October 2025
Available online 15 October 2025

namely dry and wet conditions. Ceramic nanofillers are well-renowned for enhancing the wear resistance, due to their hard and scratch-resistant nature. Few examples like titania (TiO_2) [9–11], silica (SiO_2) [12–14], silicon carbide (SiC) [15–17], silicon nitride (SiN)[18–20], tungsten carbide (WC) [21–23], and alumina (Al_2O_3) [24–26] were incorporated into EP to enhance the parent tribological properties. *Bhatia* et al. [27] incorporated boron carbide (B_4C) and silane-modified B_4C in the EP matrix and studied their tribological behaviour. The nanocomposite exhibited an abrasion mechanism, accompanied by an increase in the coefficient of friction (COF), despite a decrease in the wear rate. This phenomenon was attributed to the non-spherical shape of the nanofiller, which led to sliding rather than rolling. A decreasing trend in wear rate was noticed with increasing nanofiller content due to the obstruction offered by the nanoparticles to shear deformation during sliding. Additionally, incorporating silane-treated B_4C delayed the softening due to the stronger interaction of the silane group with the matrix. *Yang* et al. [28] reinforced EP with flower-like nickel phyllosilicate (Ni-PS) particles. The tribological tests showed that increasing the Ni-PS content enhanced the wear resistance of the system. Due to their inorganic nature, the nanofiller-reinforced matrix exhibited an abrasive wear mechanism.

SiN holds tremendous potential as an effective filler in polymer matrix, attributed to their inherent superior strength, wear resistance, fracture toughness, hardness, and creep resistance due to its strong covalent bond [29]. *Mandal* et al. [20] incorporated SiN in a polycarbonate matrix (PC) to improve the tribological properties. The nanocomposites with 20 wt % SiN showed an increment in wear resistance of 68 % and 100 % for 20 N and 25 N, respectively. These improvements are ascribed to increase in stiffness and hardness due to nanofiller incorporation. *Ramdani* et al. [30] reinforced polybenzoxazine with SiN nanofiller. The nanocomposites showed an increase by 2 GPa and 47 °C in stiffness and glass transition temperature (T_g), respectively. SiN triggers a unique mechanochemical residual curing by 'hot ball' mechanism when incorporated in room temperature cured Diglycidyl ether Bisphenol-A (DGEBA) – amine matrix and subjected to abrasive sliding.

Another ceramic nanofiller which can enhance both toughness and wear resistance of the polymer matrix is WC. They have inherent properties such as high wear resistance, fracture toughness, thermal stability, chemical stability, and strength [21]. They possess the ability to form thin carbide layers at the contact surface during abrasion sliding [31]. *Vidakis and group* incorporated WC in acrylonitrile butadiene styrene (ABS) by the material extrusion 3-D printing method. The presence of WC increased the flexural, tensile and compressive strength along with surface roughness [32]. *Al saadi* et al. [33] reinforced EP with polypropylene glycol block polyethene glycol block polyethylene glycol block structure (EO-PPO-EO) tri block copolymer (TBCP) and WC nanoparticles. A synergism was noticed between WC and TBCP, resulting in an appreciable increase in tensile and impact strength. *Kameswara reddy and group* found an increment in tensile and flexural strength for EP when incorporated with 2 wt % WC [22].

The inclusion of a single nanofiller into a polymer matrix can yield substantial improvements in specific targeted properties; however, it may also adversely affect other critical performance parameters, highlighting the need for a balanced and application-oriented design approach. Therefore, the use of hybrid fillers is being explored to impart multifunctional properties while simultaneously overcoming the limitations of single-filler system [34,35]. *Satheesan* et al. [36] reinforced EP with graphene oxide (GO) and titania to enhance the tribological properties. The hybrid nanocomposite coatings showed a modest increase in wear resistance when compared to optimized EP-GO nanocomposites, along with increased wear cycles, indicating improved stability of the coatings. *Gioti* et al. [37] utilized a dual filler system consisting of magnetite (Fe_3O_4) and barium titanate ($BaTiO_3$) to enhance the multifunctional behaviour of EP. The hybrid nanocomposites exhibited enhanced thermal stability, mechanical performance by improving tensile properties, fracture toughness, and magnetic behaviour. *Song* et al. [38] investigated the effect of heterostructured reduced graphene oxide (rGO)/ molybdenum disulfide (MoS_2) on the friction and wear behaviour of epoxy nanocomposites. The hybrid nanocomposite was synthesized by hydrothermal method, where polyvinylpyrrolidone (PVP) acted as a surfactant to promote the uniform growth of flower-like MoS_2 across the rGO surface. When incorporated into the EP matrix, the resulting nanocomposite significantly reduced the friction interface temperature, COF, and specific wear rate. These improvements are interpreted as arising from the synergistic lubrication of rGO and MoS_2, forming a stable transfer film at the sliding interface. SiN and WC have demonstrated synergistic interactions with multi-walled carbon nanotubes (MWCNTs) in dual-filler systems, resulting in hybrid nanocomposites with enhanced multifunctional properties of the polymer matrix [21,39].

This work explores the synergistic effects of a dual 0D-0D nanofiller system, SiN and WC, on the static mechanical properties, fracture toughness and wear resistance of the EP matrix. The incorporation of SiN is anticipated to enhance the crosslinking density by accelerating the curing process and promoting robust interfacial interactions between the filler and matrix. This reinforcement strategy is expected to significantly elevate the tensile strength, hardness and fracture toughness, while also improving surface-driven properties such as wear resistance and frictional performance. Furthermore, the research also includes a comprehensive analytical validation of the experimental results with the help of numerous models to strengthen the understanding of underlying mechanisms. Collectively, these results mark a significant step forward in transitioning epoxy materials from conventional engineering applications to high-performance applications across advanced technological domains.

2. Materials and methods

2.1. Materials

The Diglycidyl ether Bisphenol-A (DGEBA) epoxy resin (LY556) and Triethylenetetramine (TETA) polyamine hardener (HY951) were procured from Covai Seenu and Company, Coimbatore, India. In the dual filler system, nano Silicon Nitride (SiN) and nano Tungsten Carbide (WC), both with an average particle size of 40 nm and 99 % purity, were supplied by Ultrananotech, Bangalore, India.

2.2. Sample preparation

A LABMAN probe sonicator was used to achieve uniform dispersion of the calculated weight percentage of each nanofiller into the epoxy matrix. The sonication process was carried out for 30 min at 25 kHz. Post-sonication, the hardener was added at 15 g per 100 g of EP resin. The neat matrix, single-filler, and dual-filler systems were allowed to cure at room temperature for 72 h. After curing, the nanocomposites were machined into test specimens following ASTM standards. The sample nomenclature is provided in Table 1.

Table 1
Sample Nomenclature of EP-based single-filler and dual-filler systems.

Sn. No	*EP / SiN / WC (wt %)*	*Sample code*
1	EP / 0.25/ 0	ES1
2	EP / 0.5/ 0	ES2
3	EP/ 0/ 0.25	EW1
4	EP/ 0/ 0.5	EW2
5	EP/ 0/ 1.0	EW4
6	EP/ 0.25/ 0.25	ESW1
7	EP/ 0.25/ 0.5	ESW2
8	EP/ 0.25/0.75	ESW3
9	EP/ 0.5/ 0.25	ES2W1
10	EP/ 0.5/ 0.5	ES2W2

2.3. Characterization techniques

The tensile properties were measured using a TINIUS OLSEN H25KT (UK) universal testing machine (UTM), following ASTM D3039 standard (rectangular specimen with dimensions 100×10×3 mm). The crosshead speed was fixed at 5 mm /min, with a gauge length of 50 mm. Five samples were tested for each composition, and the average values are reported. The fracture toughness was evaluated using UTE-40 FIE UTM by Mode-I Single-Edge Notch Bending (SENB) test, according to ASTM D5045 by three-point bending mode. The applied load and crosshead speed were 20 kN and 1 mm/ min, respectively. A crack of 2 mm length was initiated to assess the crack propagation resistance. Five specimens from each formulation were tested, and the average values are reported.

The Shore D hardness test was performed using an EXCEL, Kerala durometer according to ASTM D2240 standards. Measurements were taken at three different points on the surface of each sample to account for local variations, and the average of these values was reported. The tribological tests were conducted under dry sliding conditions and were carried out using a Pin-on-disc tribometer (TR-20LE-PHM-200, DUCOM, India) at a constant rotational speed of 100 rpm for 5 min, under various loading conditions (25 N, 50 N, 100 N). The sliding distance was kept constant, i.e., 2514 m. The test samples were prepared as per ASTM G99 standards. The counterface disc, fabricated from EN-31 high carbon alloy steel, had a diameter of 168 mm and a thickness of 8 mm. The composition of the alloy included 0.9 – 1.2 wt % C, −0.1 – 0.35 wt % Si, 0.3 – 0.75 wt % Mn and 1- 1.6 wt % Cr.

A ZEISS Gemini SEM 300 Field Emission Scanning Electron Microscope (FE-SEM), Germany, was used to examine the fracture and worn surfaces of the composite specimens. Before imaging, the samples were gold-coated using a QUORUM Q150R S sputter coater. To quantitatively evaluate the fracture surface morphology and wear characteristics of the specimens, the respective SEM images were analyzed using ImageJ software (NIH, USA) [40]. The images were converted to 8-bit grayscale to enhance contrast and eliminate background noise.

The dispersion of nanofillers in the matrix was analyzed using a JEOL JEM-2100 high-resolution transmission electron microscope (HR-TEM) operated at an acceleration voltage of 200 kV. For analysis, ultrathin sections of the specimens were cryo-cut at −100 °C with a Leica FC7 ultra-microtome and subsequently mounted on copper grids for observation.

3. Results and discussion

3.1. Tensile test

The stress-strain curves under uniaxial tensile loading for neat EP, single-filler epoxy nanocomposites and epoxy hybrid nanocomposites are illustrated in Fig. 1. The tensile strength (MPa), elastic/ Young's modulus (GPa) and elongation at break (%) for EP systems reinforced with single-filler and dual-filler systems are reported in Tables 2 and 3, respectively.

From the stress-strain curves for the single filler system shown in Fig. 1a, it is apparent that both SiN and WC improve the tensile strength, Young's modulus and strain at break of the epoxy matrix. For the SiN-reinforced single-filler EP system, the ES2 sample exhibited significant improvements in mechanical properties, with increases of 222 % in tensile strength, 155 % in Young's modulus, and 174 % in strain at break, respectively. These enhancements are attributed to the formation of secondary interactions - hydrogen bonds between EP and SiN[39]. SiN is known to promote increased crosslinking density within the EP network at room temperature [41,42]. This densified crosslinked structure contributes directly to the elevated mechanical improvements by effectively resisting deformations and delaying the onset of fracture under tensile loading. The enhanced crosslinking density generates a compact 3-D polymer network that can effectively resist chain slippage, and thus demands higher stress to induce fracture. Under loading, the uniformly dispersed SiN nanoparticles facilitate stress redistribution and delay localized strain accumulation, preventing premature crack initiation. Simultaneously, the rise in Young's modulus is attributed to the restricted mobility of polymer chains and the intrinsic stiffness of ceramic SiN. The combination of higher crosslink density and homogenous filler dispersion reduces the free volume, thereby significantly constraining molecular motion within the EP matrix.

Table 2
Tensile properties of EP and single filler nanocomposites.

Samples	Tensile strength (MPa)	Young's modulus (GPa)	Strain at break (%)
EP	21.5 ± 0.8	1.1 ± 0.03	1.38 ± 0.2
ES1	65.1 ± 1.0	2.1 ± 0.3	4.01 ± 0.1
ES2	69.2 ± 0.7	2.8 ± 0.2	3.78 ± 0.2
EW1	49.7 ± 0.5	2.4 ± 0.2	3.51 ± 0.4
EW2	61.8 ± 1.2	2.6 ± 0.1	4.66 ± 0.3
EW3	53.9 ± 1.0	2.3 ± 0.3	3.71 ± 0.3
EW4	44.6 ± 1.1	1.96 ± 0.3	3.48 ± 0.1

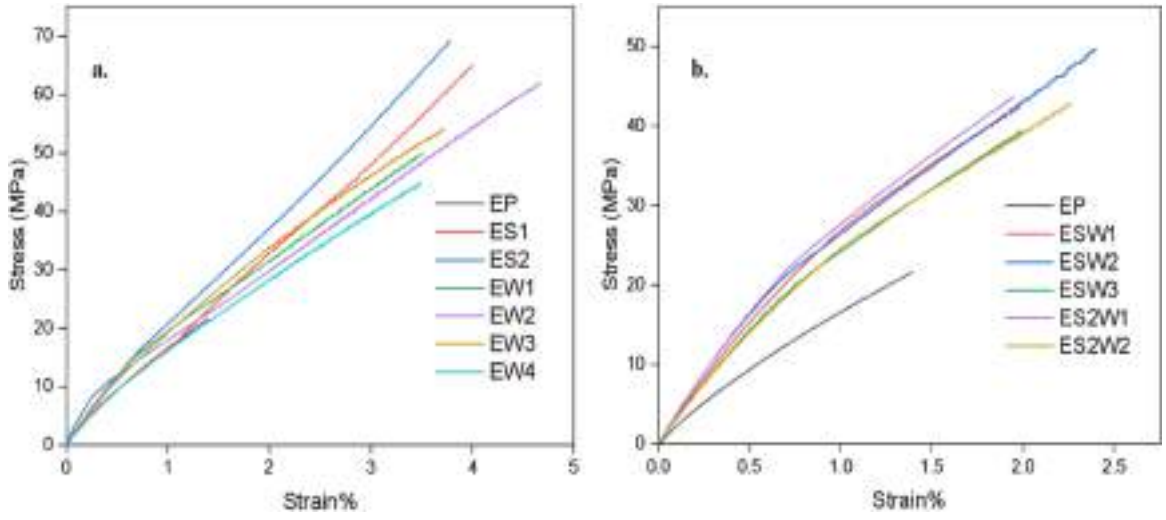

Fig. 1. Stress-strain plots of **a.)** Epoxy nanocomposites and **b.)** Epoxy hybrid nanocomposites.

Table 3
Tensile properties of dual filler nanocomposites.

Samples	Tensile strength (MPa)	Young's modulus (GPa)	Strain at break (%)
ESW1	42.3 ± 1.2	3.56 ± 0.3	1.97 ± 0.2
ESW2	49.6 ± 1.0	3.83 ± 0.1	2.40 ± 0.4
ESW3	39.3 ± 1.1	3.21 ± 0.07	1.98 ± 0.2
ES2W1	43.7 ± 0.7	3.71 ± 0.2	1.94 ± 0.3
ES2W2	42.7 ± 1.2	3.16 ± 0.1	2.26 ± 0.1

For the WC-based single-filler reinforced EP system, tensile strength, Young's modulus, and strain at break increased by 188 %, 137 %, and 238 %, respectively, for EW2. These enhancements are credited to the inherent high stiffness and strength of the WC nanofiller, which effectively transfers applied stress from the softer EP matrix to the rigid filler. WC has very high density as well (~15 g/cm^3), which contributes to higher mass-related stiffness and strength, and assists in increasing the elongation. As the filler content increased, a decline in properties was noticed, obviously due to the agglomeration of WC nanoparticles.

A mutual reinforcement effect is evident in the dual 0D-0D filler system, as shown in Table 3. For the ESW2 sample, tensile strength, Young's modulus, and strain % increased by 130 %, 248 %, and 74 %, respectively. Due to their inherent rigidity and toughness, both nanofillers facilitate efficient stress transfer between them and the EP matrix, while simultaneously restricting polymer chain mobility. This helps in minimizing stress concentration points and delays crack propagation. Their small particle size impedes the formation of microvoids, thereby decreasing potential crack propagation sites. Additionally, the dual filler system forms a heterogeneous and semi-continuous reinforcement network within the matrix, enhancing the overall mechanical integrity and load-bearing capacity of the composite.

3.2. Fracture surface analysis

The fracture surfaces of EP, ES2, EW2 and ESW2 were examined using FESEM, as shown in Fig. 2, along with microvoids. The neat EP exhibited a smooth and glassy surface, indicating minimal resistance to deformation, crack initiation and propagation[43,44]. Fig. 1a demonstrates that the incorporation of SiN enhances the ductility of the EP matrix, a result further corroborated by the FESEM image in Fig. 2b The appearance of small feather-like features indicates improved resistance to deformation, which can be attributed to the formation of secondary hydrogen bonds, as reported in previous studies [41]. Additionally, the increased crosslinking density due to SiN inclusion, combined with the reinforcing effect of the nanofiller, contributes to the suppression of crack initiation sites. In the case of ESM2 fractographs, the presence of long, well-defined river-mark patterns indicates crazing-induced plastic deformation, absent in neat EP due to its brittle nature [45]. This results in enhanced ductility and slower micro-crack propagation. These stable and ordered features suggest plastic deformation before failure, facilitated by a heterogeneous network structure that promotes uniform stress distribution. Additionally, the rigid SiN and WC fillers effectively redirect crack paths, causing the cracks to navigate around the particles and resulting in the formation of orderly ridges on the fracture surface. These ridges also signify crack arrest, accompanied by several branched micro-cracks that prevent the gradual progression of the main crack[46]. Micro void formation is significantly lower, compared to EP

3.3. Fracture toughness (SENB)

Fracture toughness is a critical parameter that defines the material's ability to resist the propagation of existing cracks under applied stress, providing insights into the structural integrity and durability, especially in the presence of defects and/or flaws. The single-edge notch bending test (SENB) is a widely used method for mode I fracture toughness. In this test, a specimen with an induced crack is subjected to load in the three-point bending mode, as shown in Fig. 3, to measure critical stress intensity factor (K_{IC}) and strain energy release rate (G_{IC}). This method enables the evaluation of various toughening mechanisms introduced by the incorporation of nanofillers, providing insights into their influence on the crack resistance and failure behaviour of polymer materials. **Eqs. 1 and 2** are used to calculate K_{IC} and G_{IC}, as given below, where B is breadth, P is load (KN), W is thickness, a is the depth of the notch, and E is Young's modulus [39].

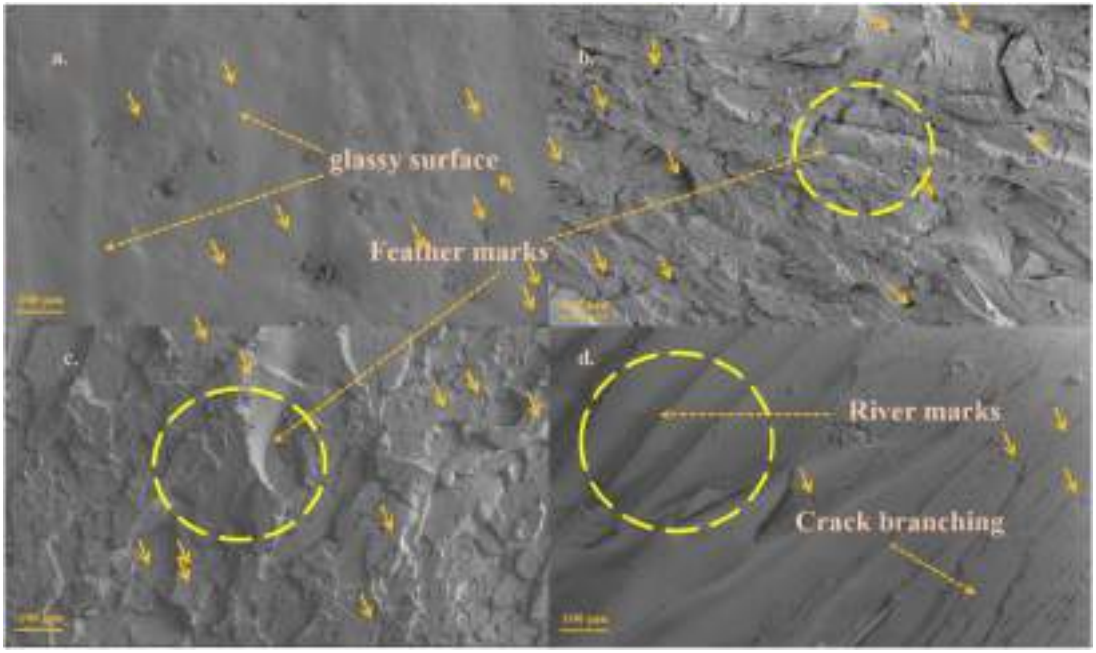

Fig. 2. FESEM images of fracture surfaces of **a.)** EP, **b.)** ES2, **c.)** EW2 and **d.)** ESW2.

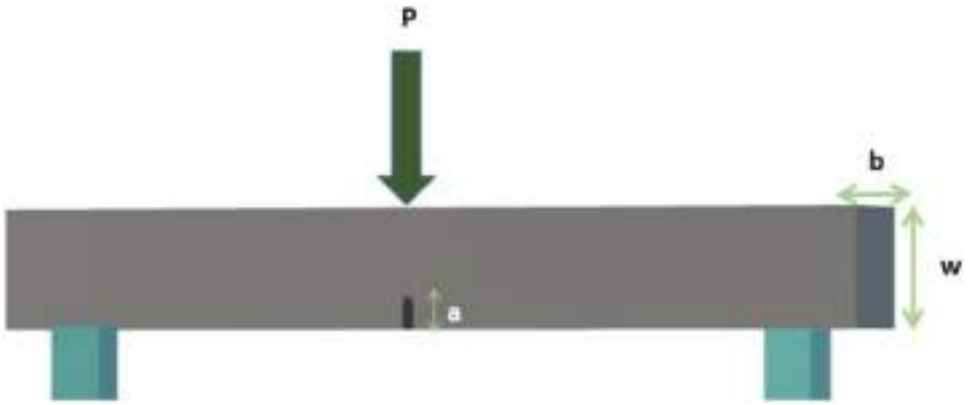

Fig. 3. Schematic representation of Single Edge Notch Bending (SENB) test (Mode I).

$$K_{IC} = \frac{4P}{B} \times \sqrt{\frac{\pi}{W}}\left(1.6\left(\frac{a}{W}\right)^{\frac{1}{2}} - 2.6\left(\frac{a}{W}\right)^{\frac{3}{2}} + 12.3\left(\frac{a}{W}\right)^{\frac{5}{2}} - 21.2\left(\frac{a}{W}\right)^{\frac{7}{2}} + 21\left(\frac{a}{W}\right)^{\frac{9}{2}}\right) \quad (1)$$

$$G_{IC} = \frac{K_{IC}^2}{E} \quad (2)$$

The neat EP exhibited K_{IC} and G_{IC} values of 2.38 MPa.m$^{1/2}$ and 5.14 kJ/m^2, respectively, as observed in Fig. 4. For single-filler nanocomposites, ES2 showed an increase of 77 % in K_{IC} and 23 % in G_{IC}, while EW2 exhibited an enhancement of 106 % in K_{IC} and 80 % in G_{IC}. The inclusion of SiN improved fracture toughness due to enhanced curing and secondary bond formation [39,41].

WC nanoparticles enhance toughness by uniformly distributing the applied stress, thereby increasing the energy required to propagate cracks [21]. WC can induce unique mechanisms - 'paperweight' effect and 'anchoring' effect, where the high-density nanoparticles act as nano paperweights within soft EP matrix by suppressing deformation around them, especially near crack tips. These particles anchor the EP layers, preventing local matrix deformation, thereby increasing the energy required for the crack to propagate. For the ESW2 hybrid nanocomposite, a 244 % and 241 % increase in K_{IC} and G_{IC} values, respectively, is observed. A synergism is noticed between the dual 0D nanofillers, where the enhanced crosslinking credited to SiN exponentially enhances the paperweight and anchoring effect displayed by WC, as shown in Fig. 5. At this composition, the fillers are well-dispersed within the matrix, enabling efficient stress transfer and energy dissipation through various mechanisms. This balanced dispersion prevents the formation of agglomerates that typically act as stress concentrators and strengthen the composite at higher loads. Dual-fillers with high overall filler content exhibit agglomeration, which limits their reinforcing efficiency.

3.3.1. *Fracture toughness modelling*

Linear Elastic Fracture Mechanics (LEFM) is a theoretical framework used to analyze the behaviour of materials containing a pre-initiated crack under applied stress, assuming linear elastic behaviour [47]. It is useful in predicting the onset of fracture in brittle or quasi-brittle materials, where plastic deformation is minimal and localized around the crack tip.

3.3.1.1. Crack tip opening displacement (COD). This section investigates the influence of 0D nanofillers on the fracture toughness of EP by using analytical models and a detailed examination of the underlying mechanisms. As a first step, the crack opening displacement (COD) is evaluated to assess the potential for crack pinning within the system, (Fig. 6a), where r_n is the radius of the nanoparticles. Crack pinning is conceptually analogous to the obstruction of dislocation motion in metals by dispersed particles [48]. By reducing the interparticle spacing and minimizing the dispersed particle size, a more effective toughening effect can be achieved, as the fillers serve as barriers to crack propagation..

Crack pinning can be identified by bowing lines on the fractured surface. *Kinloch* et al. [49] and *Dittanet and Pearson* [50] observed

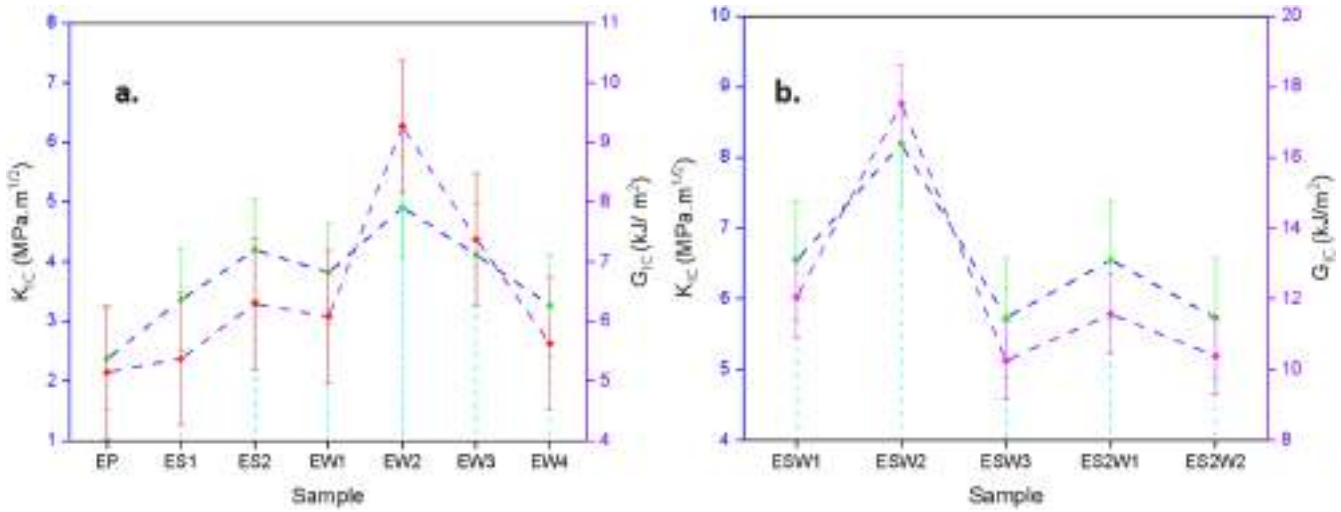

Fig. 4. Fracture toughness parameters of **a.)** epoxy nanocomposites and **b.)** epoxy hybrid nanocomposites.

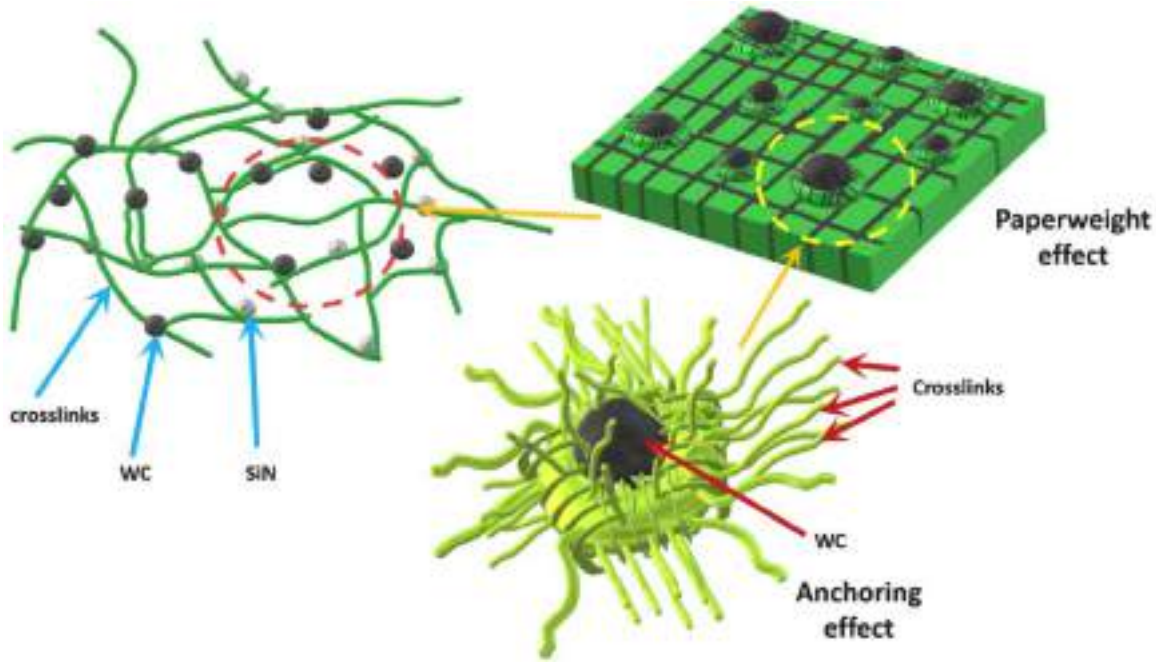

Fig. 5. Schematic representation of paperweight and anchoring effect displayed by WC when incorporated in EP matrix.

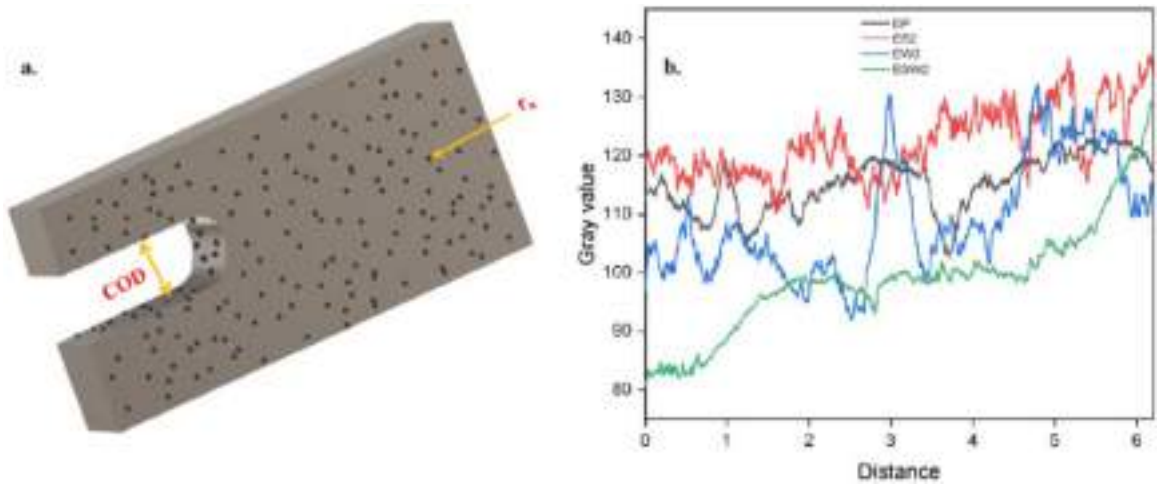

Fig. 6. a.) Crack tip opening displacement (COD) and **b.)** Fracture surface roughness.

bowing lines for EP containing micro-spherical glass beads and micro-silica, respectively, suggesting this mechanism could be prevalent in brittle EP matrices. For crack pinning to occur, the particles incorporated into the matrix should be bigger or at least equal to the COD. The COD should be calculated to confirm whether this mechanism has occurred. Under plane strain conditions, the COD can be calculated by Eq. (3), where G_{IC} is the experimentally obtained strain energy release rate and σ_y is the yield stress (0.2 % proof strain) [51].

$$COD = \frac{G_{IC}}{\sigma_y} \tag{3}$$

The calculated values are presented in Table 4. When the COD is significantly larger than the particle size, the crack front is unlikely to interact with the particles, causing the material to behave as a continuous and homogenous medium [52]. Based on the results, it is evident that the nanoparticles used- both in single and dual filler systems- are smaller than the COD (40 nm average diameter), suggesting a low probability of crack pinning or crack front bowing in these nanocomposites.

Table 4
crack opening displacement (COD), plastic radius (r_y), and crack deflection energy (ΔG_{CD}) for EP and its multi-filler systems.

Sample code	COD (mm)	r_y (mm)	ΔG_{CD} (J/m^2)
EP	0.37	1.5	–
ES2	0.31	1.9	15.2
EW2	0.50	3.4	3.07
ESW2	0.57	3.4	3.08

Neat EP, due to its brittle nature, exhibits limited COD, reflecting its inability to undergo significant plastic deformation near the crack tip. In the case of ES2, increased crosslinking density contributes to reducing COD relative to EP, as the enhanced stiffness and rigidity restrict large-scale deformation near the crack tip region. Conversely, the incorporation of WC nanoparticles in EW2 and ESW2 results in higher COD

compared to EP. This increase is attributed to the 'anchoring' and 'paperweight' effect, as shown in Fig. 5. These mechanisms may contribute to improved fracture toughness primarily through crack deflection rather than direct crack pinning.

3.3.1.2. Crack path deflection. The toughening effect imparted by reinforcements in a polymer matrix has been extensively described by Faber and Evans [53,54]. According to their model, the presence of hard and rigid particles alters the crack trajectory, causing it to tilt and twist out of its original propagation plane. This crack deflection mechanism leads to an increase in the overall fracture surface area, thereby enhancing the fracture energy of the material. The additional energy for crack deflection (ΔG_{CD}) is estimated using Eq. (4), where γ_m is the specific fracture energy of an unfilled matrix, corresponding to the mode I G_{IC} of EP, and V_f is the volume fraction of the nanofillers [52]. The calculated values are provided in Table 4.

$$\Delta G_{CD} = \frac{3}{2} \times \gamma_m \times V_f \tag{4}$$

The calculated ΔG_{CD} for the nanocomposites are relatively small in comparison to the overall fracture toughening contributions, indicating that crack deflection has a very minor role to play in this case. This is primarily because the nanoparticles are significantly smaller than the micron-scale crack tip, limiting their ability to alter the crack path effectively. Among the samples, ES2 exhibited the highest crack deflection energy, which is attributed to the increased crosslinking density, making crack deflection more favourable over blunting or direct propagation. In contrast, WC-based nanocomposites demonstrated negligible ΔG_{CD}, suggesting minimal contribution of WC on crack deflection.

3.3.1.3. Radius of plasticity (r_y). Another way to understand the influence of nanofillers on the brittle matrix is by calculating its radius of plasticity (r_y). The plastic zone radius is the distance from the crack tip over which the material yields plastically due to high stress concentrations, as shown in Fig. 7b Irwin proposed a model to determine the size of the plastic zone ahead of the crack tip, according to LEFM [55], using Eq. (5), which is presented in Table 4.

$$r_y = \frac{1}{6\pi} \times \left(\frac{K_{IC}}{\sigma_y}\right)^2 \tag{5}$$

The slope obtained by plotting the measured plastic zone size (r_y) vs (K_{IC} / σ_y^2) is found to be 0.05, which closely aligns with the theoretical value predicted by Irwin's model, $1/6\pi \approx 0.053$, as depicted in Fig. 13a. This strong correlation confirms the validity of the experimental measurements and supports the role of the plastic zone in contributing to the overall toughening mechanism of the nanocomposites.

ES2 exhibited a 27 % increase in plastic zone radius compared to EP, which was the lowest among all nanocomposites due to the enhanced stiffness and crosslinking density, restricting large-scale plastic deformation. EW2 demonstrated a significant 127 % increase, primarily due to the 'anchoring' and 'paperweight' effect. These dense nanofillers act like local weights, impeding matrix displacement and creating energy dissipation zones. As a result, the crack tip encounters greater resistance, requiring more energy to propagate, which promotes localized plastic deformation and subsequently enlarges the plastic zone radius. ESW2 displayed a similar enhancement, further confirming that the toughening mechanism governed by plastic zone expansion is predominantly influenced by the presence of WC nanoparticles.

3.3.1.4. Huang and Kinloch model. The toughening model developed by Huang and Kinloch defined the overall toughening contribution (ψ) as a combination of two primary mechanisms: localized plastic shear banding (ΔG_S), typically resulting from the bridging effect, and plastic void growth (ΔG_v), which arises from debonding or cavitation of the nanoparticles. In the present study, the rigid spherical nanoparticles did not exhibit any evidence of bridging behaviour, as confirmed by the fracture micrographs in Fig. 2. This suggests that localized shear banding is unlikely to play a significant role[51]. Therefore, for subsequent calculations, the toughening contribution is considered to arise predominantly from the plastic void growth mechanism. The respective contributions are evaluated using Eq. (6–7) [56].

$$G_{IC} = G_{Im} + \Delta G_v \tag{6}$$

$$\Delta G_v = \left(1 - \frac{\mu_m^2}{3}\right) \times (v_v - v_f) \times \sigma_{yc} \times r_{yu} \times K_{vm}^2 \tag{7}$$

Where, G_{Im} is the strain energy release rate of unfilled matrix, ΔG_v is the toughening contribution by plastic void growth, μ_m is a material constant related to von Mises yield criterion, taken ≈ 0.2. K_{vm} is the maximum stress concentration factor of the von Mises stress in the plastic matrix, found to be around 2.22 around a void in an epoxy matrix [51]. σ_{yc} is the yield compressive strength, which can be found by dividing tensile yield by 0.7, according to ASTM [57], and v_v and v_f are the volume fractions of voids and the volume fraction of particles, and r_{yu} is the radius of the plastic zone for unfilled epoxy matrix.

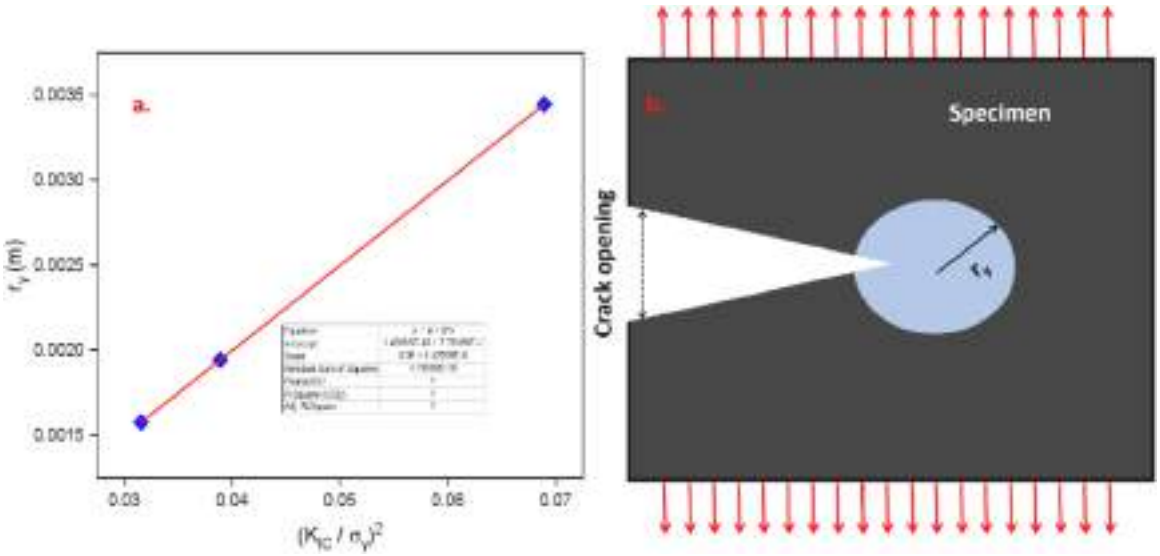

Fig. 7. a.) Measured plastic zone size (r_y) vs (K_{IC} / σ_y^2) and **b.)** Radius of plasticity (r_y) in polymer specimen.

Table 5
Huang and Kinloch theoretical G_{IC} prediction, experimentally obtained G_{IC}, and surface roughness.

Sample code	Theoretical G_{IC} (kJ/m^2)	Experimental G_{IC} (kJ/m^2)	Surface roughness (R_a)
EP	5.1	5.1	3.87
ES2	6.1	6.3	5.23
EW2	7.6	9.2	8.18
ESW2	9.4	17.5	7.1

Table 5 shows that the Huang and Kinloch model provides an accurate prediction for ES2, indicating the dominance of plastic void growth in the nanocomposite. However, the model underestimates the fracture toughness for WC-containing single and dual filler systems. WC contributes to the toughening process through additional mechanisms beyond void growth, as discussed previously, suppressing matrix deformation and increasing energy absorption near the crack tip. Since these mechanisms are not incorporated in the original model, the experimentally observed fracture toughness values exceed the theoretical predictions.

3.3.1.5. Surface roughness (R_a). The surface roughness (R_a) values obtained by analyzing FESEM fracture images using ImageJ are tabulated in Table 5, along with crack roughness and surface plots, as shown in Fig. 6b and 8. The 3D plots revealed distinct differences in surface features in EP and nanocomposite samples. EP showed a comparatively smoother and flat surface plot, characteristic of brittle failure. This is further supported by the fracture SEM image and the lowest surface roughness value recorded, which collectively indicate the inability of the material to yield and a lack of appreciable energy absorption before fracture. In contrast, the nanocomposites showed significantly rougher and more tortuous fracture surface features. These are manifestations of increased fracture surface area and complex crack propagation paths, which are commonly associated with various toughening mechanisms, such as microcrack deflections, enhanced plastic deformation zones, among others. ES2 increased surface roughness by 35 % compared to EP, attributed to improved crosslinking density and microcrack branching mechanisms. EW2 showed pronounced enhancement, with a 111 % rise in R_a, pointing towards extensive plastic deformation and strong interaction between the crack front and WC nanoparticles. Similarly, ESW2 showed an 84 % increase, reflecting synergistic effects from both SiN and WC. These enhancements are consistent with the paper weight and anchoring effects, as discussed earlier. Overall, the increased surface roughness observed in the nanocomposites directly correlates with enhanced energy dissipation mechanisms, supporting the hypothesis that the nanofillers not only modify the crack path but also significantly improve the fracture resistance of EP. The combined evidence from 3D surface plots, surface roughness, and FESEM fractographs indicates that the addition of nanofillers fundamentally alters the failure mode of EP, transitioning from a brittle to a semi-ductile fracture behaviour.

3.4. Hardness

Fig. 9 presents the shore D hardness values of EP, single-filler, and dual-filler nanocomposites. Among the single-filler composites, ES2 exhibited superior hardness with a 21 % increase, attributed to its enhanced crosslinking, which increases the resistance to indentation. EW2 also showed a notable 16 % improvement due to the intrinsic hardness of the ceramic WC nanoparticles. The dual-filler composite, ESW2, demonstrated the highest increase at 24 %, indicating a synergistic interaction between the nanofillers and the matrix, resulting in superior hardness.

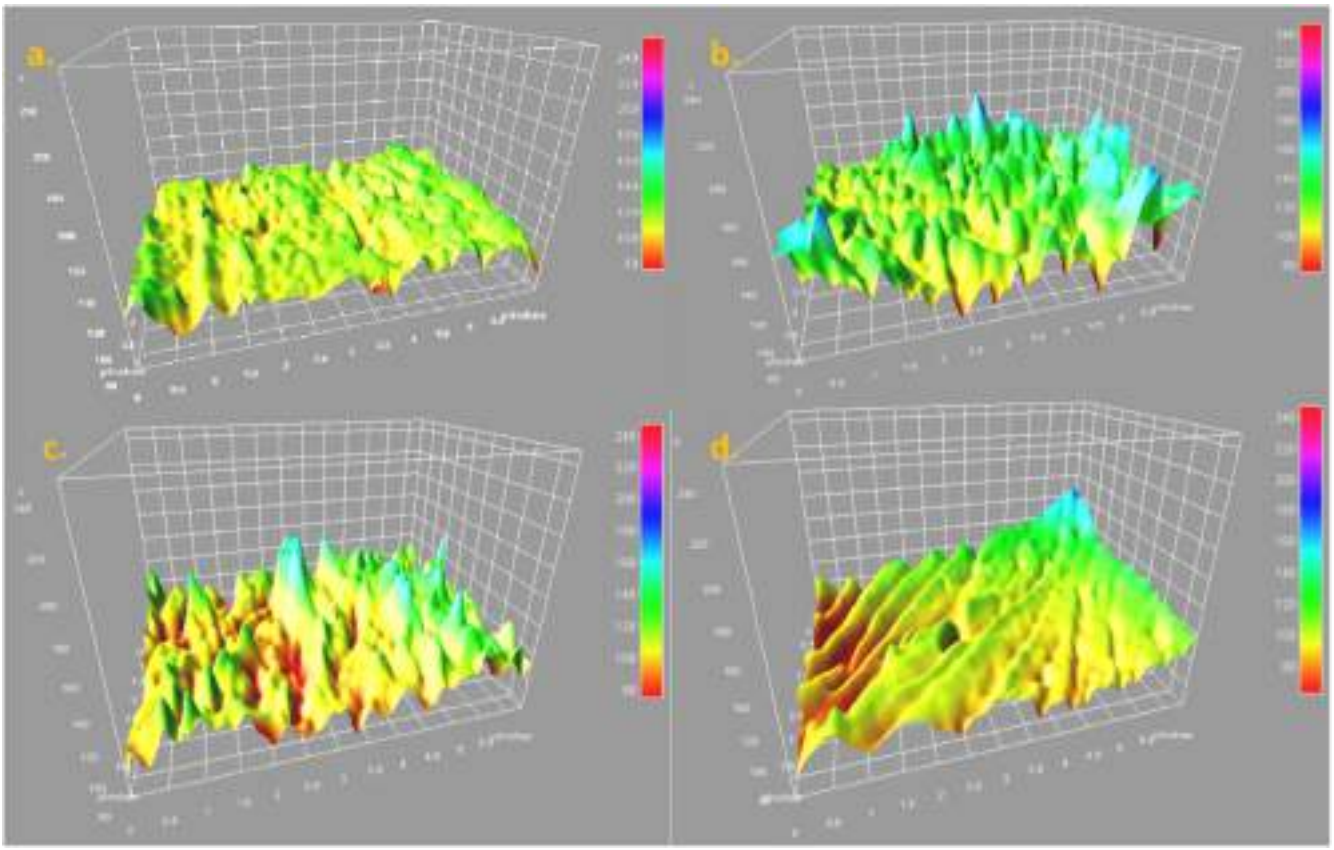

Fig. 8. I. Surface plots and **II.** 3D surface plots of **a.)** EP, **b.)** ES2, **c.)** EW2, and **d.)** ESW2.

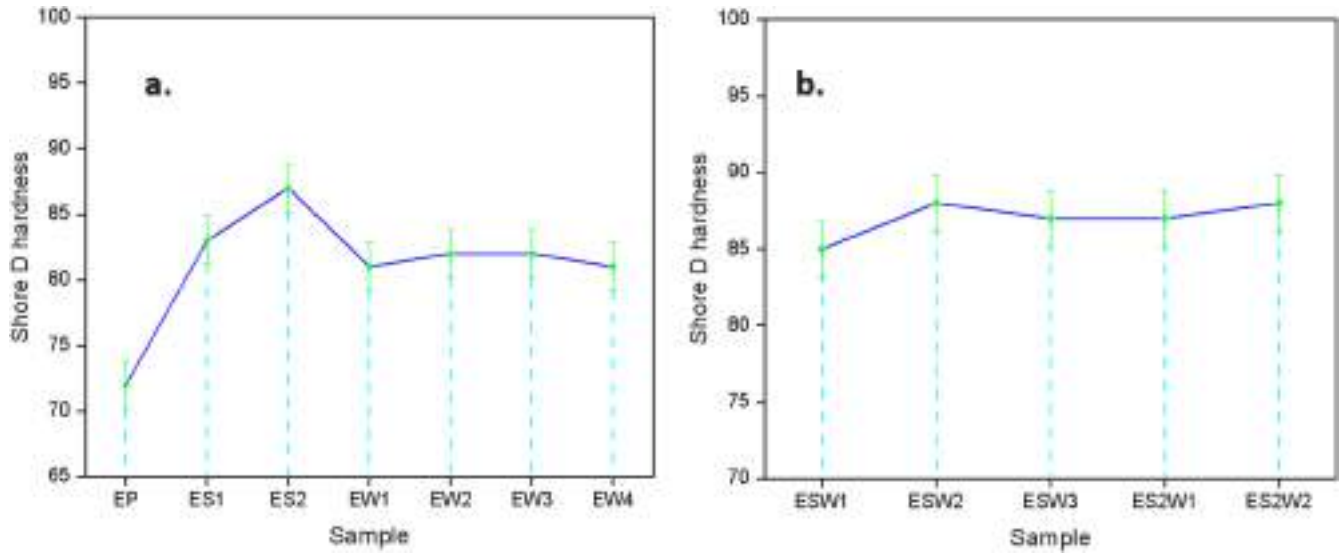

Fig. 9. hore D hardness for **a.)** epoxy single-filler nanocomposites and **b.)** epoxy dual-filler nanocomposites.

3.5. Tribology

Polymer wear refers to the gradual mass removal from the polymer surface as a result of frictional contact with a harder and rougher counterface. Unlike metals and ceramics, polymers exhibit complex wear mechanisms influenced by their viscoelastic nature, molecular structure, low surface energy, and surrounding conditions like temperature and humidity [58].

Polymers typically exhibit four primary modes of wear: adhesive, abrasive, surface fatigue, and tribochemical wear. Abrasive wear dominates when rough surfaces or hard particles slide against the polymer, leading to material removal through cutting or ploughing actions. Adhesive wear involves the transfer of material between contacting surfaces, often resulting in the formation of transfer films on the counterface [59,60]. Surface fatigue arises from repeated cyclic stresses at the contact interface, which induce the initiation and propagation of micro-cracks, eventually material loss. In contrast, tribochemical variety is driven by chemical reactions at the polymer surface, triggered by wear and environmental factors such as oxygen, moisture, etc. This leads to the breakdown of molecular chains and surface embrittlement, accelerating wear under service conditions [61,62]. The load applied during the wear process is crucial as it directly influences the frictional heat generated, which overall influences the softening of EP. This section investigates the effect of varying loads (25 N, 50 N and 100 N) on the tribological behaviour of epoxy, single-filler systems and dual-filler systems.

The specific wear rate is determined using Eq. (8).

$$Specific\ wear\ rate = \frac{mass\ loss\ (g)}{load\ (N) * sliding\ distance\ (m)} \quad (8)$$

Under repeated rotational movement of the counterface, the polymer layers experience continuous shear, which can significantly compromise their structural ability. This intense motion may cause the shearing of horizontally oriented polymer layers, leading to rupture of covalent bonds and eventual material failure [63]. The integrity of the polymer under such conditions depends largely on the strength of intermolecular bonds- stronger bonding improves resistance to deformation. However, due to the inherently brittle nature of EP, inefficient stress distribution can accelerate wear and crack propagation. To mitigate these issues, the incorporation of ceramic nanofillers- specifically spherical 0D nanoparticles- has proven highly effective. These nanofillers, known for their intrinsic hardness and thermal conductivity, enhance wear resistance by strengthening the matrix and minimizing inter-particle spacing [64]. This densification restricts polymer chain mobility and enhances the composite's ability to withstand mechanical stress and thermal buildup, ultimately improving its tribological performance.

Table 6
Specific wear rate and steady state COF for epoxy, single-filler and dual-filler nanocomposite systems.

Sample code	25 N - Specific wear rate * 10–8 (g/Nm)	25 N - COF	50 N - Specific wear rate * 10–8 (g/Nm)	50 N - COF	100 N - Specific wear rate * 10–7 (g/Nm)	100N-COF
EP	30.87± 2.3	0.62 ± 0.09	165.91± 3.1	0.34 ± 0.1	21.22 ± 3.0	0.18
ES1	3.50± 1.1	0.66 ± 0.02	4.13± 1.5	0.68 ± 0.02	4.39 ± 1.1	0.39 ± 0.11
ES2	3.02± 0.9	0.72 ± 0.03	3.42± 1.2	0.64 ± 0.04	3.82 ± 1.4	0.31 ± 0.03
EW1	4.45± 0.8	0.65 ± 0.02	4.77± 1.4	0.62 ± 0.01	4.89 ± 1.1	0.23 ± 0.03
EW2	3.34± 0.8	0.64 ± 0.02	2.70± 1.6	0.60 ± 0.03	3.79 ± 0.8	0.20 ± 0.04
EW3	4.12± 1.3	0.66 ± 0.04	3.67± 1.4	0.61 ± 0.02	4.13 ± 1.6	0.21 ± 0.03
EW4	5.21± 1.1	0.67 ± 0.03	4.94± 1.8	0.62 ± 0.02	5.21 ± 1.3	0.21 ± 0.05
ESW1	3.66± 1.7	0.69 ± 0.06	4.37± 1.3	0.62 ± 0.04	3.48 ± 1.4	0.17 ± 0.03
ESW2	3.18± 1.4	0.65 ± 0.04	2.46 ± 1.2	0.55 ± 0.05	1.46 ± 1.1	0.21 ± 0.06
ESW3	3.34± 1.6	0.67 ± 0.06	3.66± 0.9	0.61 ± 0.02	3.24 ± 1.3	0.22 ± 0.02
ES2W1	6.23± 1.9	0.63 ± 0.02	6.12± 1.2	0.41 ± 0.03	4.75 ± 1.5	0.19 ± 0.04
ES2W2	6.98± 1.4	0.65 ± 0.04	6.65 ± 1.4	0.38 ± 0.04	4.79 ± 1.0	0.18 ± 0.05

3.5.1. Wear analysis

The specific wear rates, as shown in Table 6, ascertain the positive role of 0D nanofillers on the wear resistance of the EP matrix. For wear results at 25 N load, out of all the samples, ES2, EW2, and ESW2 displayed the best wear resistance, with increments of 91 %, 89 %, and 90 %, respectively. This enhancement can be credited to the increased resistance to shear during cyclic sliding. The incorporation of SiN has drastically improved the wear resistance of EP, as supported by previously reported work [18,41]. WC has inherently very high hardness and wear resistance, which contributes to the reduction in wear rate of EP nanocomposites [65]. Furthermore, they can resist shear deformation during cyclic sliding. ESW2 exhibited a combination of the beneficial properties of SiN and WC, indicating a synergistic interaction between the fillers and EP. As the load applied is low, the frictional heat generated is minimal and does not significantly affect the material's behaviour. Under these conditions, the inherent wear-resistant properties of the nanofillers become the dominant factor influencing the overall tribological performance of the composite.

At elevated loads, i.e. at 50 N and 100 N, frictional heat becomes a crucial factor affecting the performance of polymers. Due to their inherently low thermal stability, characterized by a low melting point (T_m) and glass transition temperature (T_g), polymers are highly susceptible to thermal softening under such conditions. The heat generated at the sliding interface can soften the matrix, leading to increased mass loss. Hence, it is crucial not only to improve the wear resistance but also to enhance the thermal properties of the polymer composite to ensure stability and durability under high-load applications.

At an applied load of 50 N, ES2, EW2, and ESW2 exhibited improvements of 98 %, 98.3 % and 99 %, respectively, as observed from Table 6. When the load was increased to 100 N, the enhancements observed for ES2, EW2 and ESW2 are 82 %, 83 % and 94 %, respectively. SiN is known for its excellent thermal storage capacity and significant thermal conductivity, as reported in earlier studies[66–68]. Under dry abrasive sliding conditions, SiN demonstrates a unique 'hotball' mechanism, wherein the friction-generated heat is absorbed by SiN nanoparticles, effectively acting as thermal reservoirs or 'hotballs'. This localized heating initiates residual curing within the room-temperature-cured epoxy matrix, promoting additional crosslinking of unreacted monomers [69]. As a result, the contact surface experiences enhanced hardness and improved thermal stability. This amplification can be directly correlated to increased wear resistance at higher loads (50 N and 100 N). WC exhibits high thermal conductivity owing to its stable ceramic structure [70], which enables more efficient dissipation of frictional heat generated, reducing localized thermal softening and helping preserve the structural integrity of the EP matrix. In the case of ESW2, a synergistic effect is observed between the two nanofillers. The increased crosslinking induced by SiN, combined with the additive thermal conductivities of both 0D ceramic nanofillers, leads to a significant improvement in wear resistance, particularly under higher loads.

3.5.2. Coefficient of friction (COF)

The coefficient of friction is determined by calculating the ratio of the tangential force, specifically the frictional force, to the normal force acting on the surface when the specimen and the counterface are in contact during relative motion. It measures the resistance to motion between two surfaces and is a critical parameter in understanding the tribological behaviour of polymers. It is heavily influenced by a range of factors such as surface roughness, contact pressure, sliding speed, temperature, and material properties. Unlike metals and ceramics, polymers exhibit viscoelastic behaviour, making the frictional response more complex and sensitive as the heat generated during friction can soften the matrix and thereby reduce the resistance to sliding. When friction combines with high compressive force and rotational speeds, a substantial temperature rise is noticed between the contact surface and counterface.

At a loading condition of 25 N, the COF shows minimal variation, as seen in Fig. 10a and Table 6. This consistency in COF can be attributed to the relatively low compressive load, which generates minimal frictional heat at the contact interface. Accordingly, material softening is limited, maintaining stable sliding conditions which reduces fluctuations in frictional behaviour. For 50 N loading conditions, a fluctuating coefficient of friction (COF) can be observed for the EP sample (Fig. 10b), indicating rapid surface deterioration and eventual failure. The frictional heat generated due to the increased compressive force is considerable, resulting in softening of the unfilled material. ES2 exhibited stability in COF, with a steady-state COF of 0.64 (an 88 % increase), indicating thermal stability near the contact surface. The enhanced crosslinking, along with the higher thermal storage capacity of SiN, is the primary reason for this unique phenomenon.

EW2 demonstrated stable COF by quickly attaining steady state region, with a slightly lower COF than ES2. This non-fluctuating COF in EW2 can be attributed to the rolling effect of WC nanoparticles, which facilitates smooth sliding against the counterface [71]. Owing to their spherical morphology, these nanoparticles function like 'micro ball bearings' at the sliding interface, reducing direct shear interactions between the mating surfaces by partially converting sliding motion into rolling, as shown in Fig. 12. Additionally, WC's high hardness and excellent thermal conductivity help to preserve surface integrity under applied compressive load. In comparison, ESW2 showed an even lower and highly stable COF, a result of synergistic interaction between SiN's hotball effect – enhancing crosslinking and surface hardening- and WC's micro ball bearing mechanism, collectively improving frictional stability and wear performance.

At 100 N applied load, appreciable frictional heat is generated, leading to softening of the EP matrix which facilitates easier sliding. As a result, EP exhibited the shortest running-in period and rapidly reached the lowest COF due to extreme matrix softening, though this also contributed to its high wear rate, as indicated in Table 4. In contrast, ES2 showed the longest running-in period, attributed to the need for initial surface adaptation. The increased crosslinking and surface hardness from SiN led to greater surface roughness, causing abrasive interactions such as micro-cutting, ploughing, thereby delaying stabilization. EW2 exhibited a shorter running-in period than ES2, crediting the micro ball-bearing effect of spherical WC nanoparticles. These particles helped reduce interfacial shear and promoted quicker stabilization under load. Among all the nanocomposites, ESW2 achieved the fastest transition to steady-state COF, crediting the synergistic interaction between SiN's surface reinforcement and WC's rolling behaviour, enabling rapid surface conditioning and enhanced tribological stability.

3.5.3. Worn-out surface analysis

FESEM is a powerful tool widely employed for surface analysis of worn polymers and their composites. During abrasive sliding, polymers undergo complex wear mechanisms, leading to distinct morphological changes on the surface. This section provides a detailed examination of the influence of varying applied loads on the morphology of the worn surfaces.

3.5.3.6. Worn surface at 25 N loading. Fig. 11 presents the FESEM micrographs of the worn surfaces for EP, ES2, EW2 and ESW2 nanocomposites under an applied load of 25 N. Despite the relatively low applied load, EP exhibited noticeable surface damage, corroborated by the significant mass loss and higher COF, as reported in Table 6 **and** Fig. 10a. This behaviour can be attributed to the complex 3-D network formed during curing, which limits its ability to resist shear forces. The resulting high COF leads to matrix softening and accelerated wear, and finally, surface damage. ES2 exhibited a dominant abrasive wear mechanism, attributed to increased surface hardness and high resistance to deformation. These properties led to micro-cutting and ploughing of the softer EP matrix during sliding. In contrast, EW2 demonstrated a

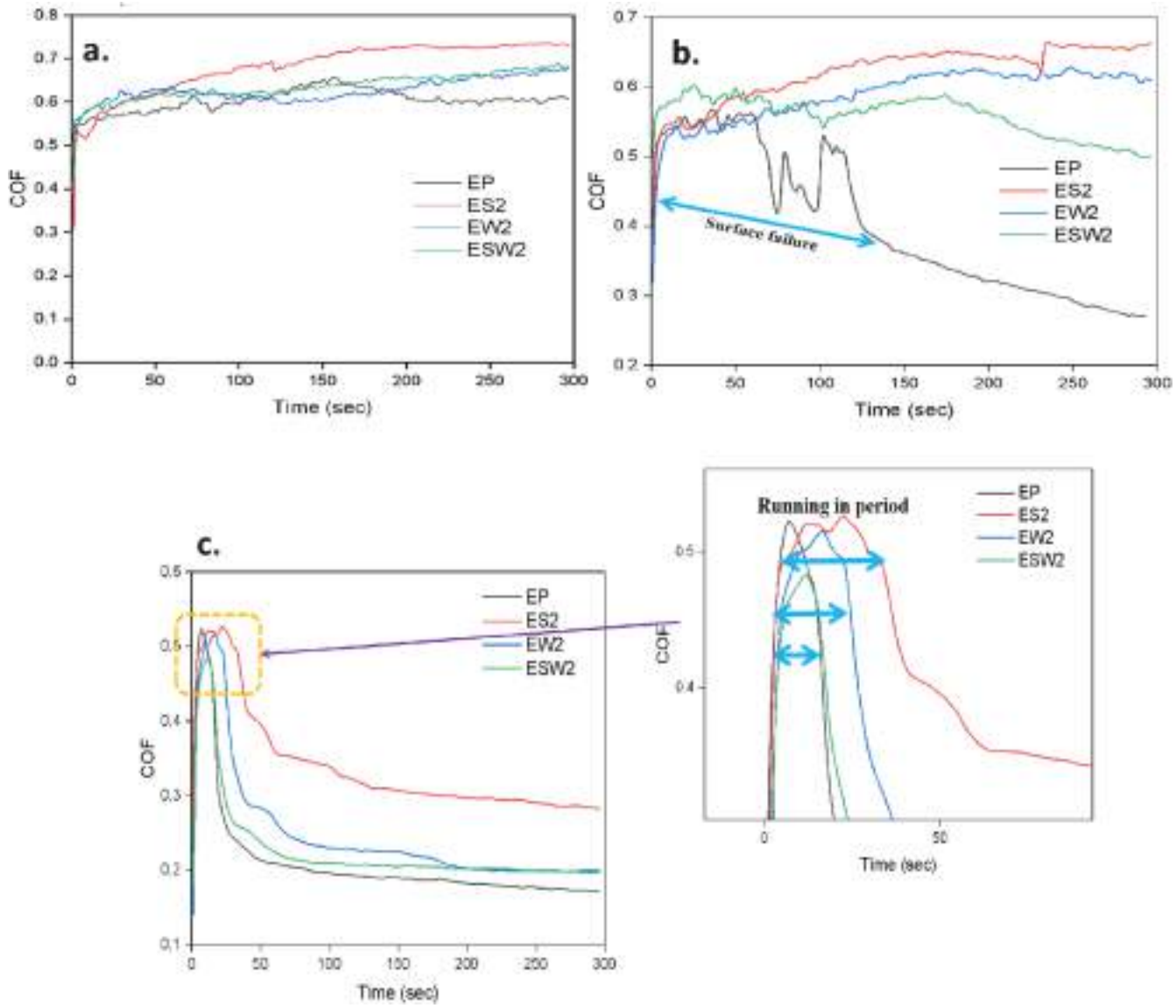

Fig. 10. Coefficient of friction plots for loads at **a.)** 25 N, **b.)** 50 N, and **c.)** 100 N.

combination of ploughing and transfer film formation. While the ploughing behaviour was comparable to that of ES2, the presence of spherical WC nanoparticles introduced a distinct effect, where they act like 'spacers' between the counterface and the specimen surface, reducing adhesive interactions at the interface. Due to their mobility within the matrix, the WC nanoparticles tend to redistribute during ploughing, facilitating the development of transfer films on the contact surface. This mechanism led to a more gradual, delayed and controlled material loss, as reflected in the wear data presented in Table 6. A similar wear mechanism is observed in the case of ESW2; however, the presence of both SiN and WC nanoparticles imparted a synergistic effect. The combined presence of these two 0D nanofillers led to a balanced wear response, with WC enabling smoother sliding and transfer films and SiN enhancing surface hardness and thermal stability. The synergistic interaction resulted in improved wear resistance compared to the single-filler systems, as the nanofillers worked in tandem to both reduce direct shear contact and reinforce structural integrity of the matrix.

3.5.3.7. Worn surface at 50 N loading. Fig. 13 presents the worn surface micrographs for EP, ES2, EW2, and ESW2 under an applied load of 50 N. As observed from Table 6 **and** Fig. 10b, EP experienced severe wear and significant matrix softening, as evident from the substantial material accumulation and smearing visible in Fig. 13a. The thermal softening of the matrix under higher load minimized the resistance to sliding, and distinct plough marks were absent and facilitated easy material removal. In contrast, ES2 exhibited prominent abrasive plough marks, a result of its increased surface hardness and resistance to deformation. These characteristics, combined with the higher COF observed, confirm the abrasive wear mechanism governing ES2's surface behaviour under the given load. Similar to the behaviour observed under the 25 N load, EW2 continued to exhibit both ploughing and transfer film formation under 50 N condition. In addition, several smoother regions were evident on the worn surface, attributed to the nano-polishing effect and rolling behaviour of hard WC nanoparticles [72], as shown in Fig. 12. These nanoparticles act as a third body at the sliding interface, initiating an abrasion polishing mechanism [71]. During frictional sliding at higher loads, the embedded WC nanoparticles function as abrasive or micro-brushing agents, gradually smoothing the polymer surface at the nanoscale. This nano-polishing action not only reduces surface roughness but also contributes to lower COF by facilitating easier sliding. Furthermore, the polished surface promotes the formation of a relatively continuous and adherent transfer film, improving tribological stability.

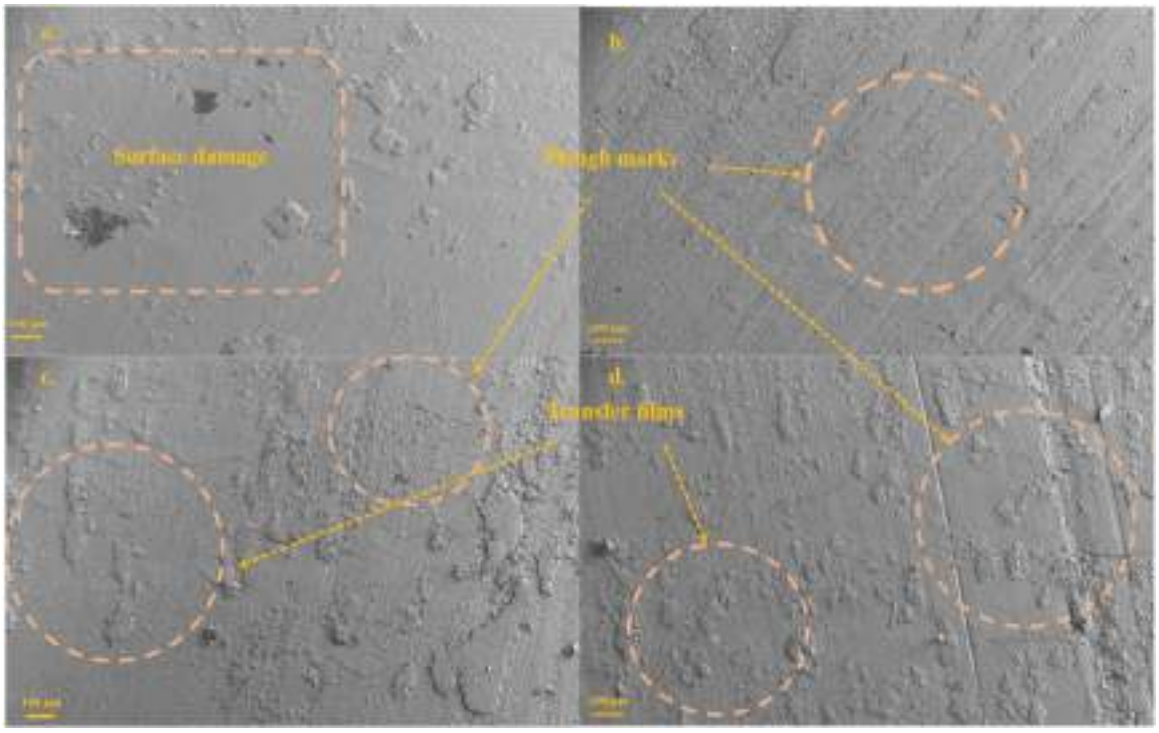

Fig. 11. FESEM images for worn-out surfaces of **a.)** EP, **b.)** ES2, **c.)** EW2, and **d.)** ESW2 at 25 N applied load.

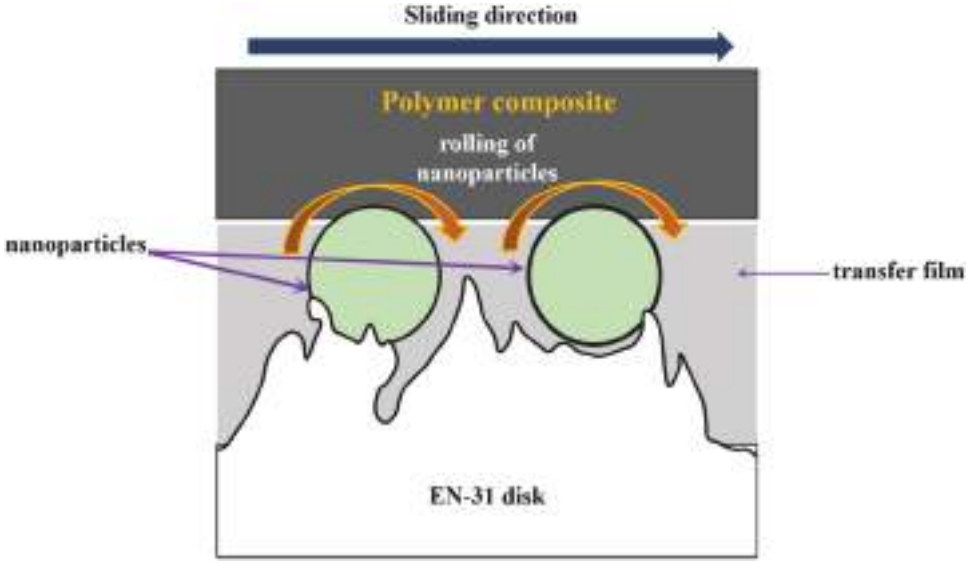

Fig. 12. Rolling behaviour of WC nanoparticles embedded in EP matrix.

These effects are reflected in the steady state behaviour shown in Fig. 10 and the uniform transfer layer observed in Fig. 13c.

These integrated effects are observed clearly for ESW2, as shown in Fig. 13d The surface displays smoother regions attributed to the nano-polishing and rolling action of WC, along with distinct plough marks resulting from the abrasive action of SiN, indicating synergism between fillers even at higher load.

3.5.3.8. Worn surface at 100 N loading. At elevated loads, thermal stability becomes critically important, as the high compressive forces can generate substantial frictional heat at the contact interface. Under extreme loading conditions (100 N), a noticeable shift in wear mechanism is observed when compared to lower loads, as illustrated in Fig. 11. EP exhibited severe surface damage, highlighting its inability to withstand thermal softening, which led to significant material degradation. In contrast, ES2 continued to exhibit a ploughing mechanism (abrasion), even under these harsh conditions, demonstrating superior thermal stability. This behaviour can be attributed to the residual curing effect induced by SiN nanofillers through the 'hot ball' mechanism, which enhances crosslinking and strengthens the surface.

Interestingly, both EW2 and ESW2 showed minimal evidence of ploughing and instead presented smoother worn surfaces and well-developed transfer films, indicating the dominance of nano-polishing at elevated loads. At such high loads, the increased frictional force facilitates deeper embedding and more active participation of WC nanoparticles over SiN at the sliding interface. This dominance of WC is due

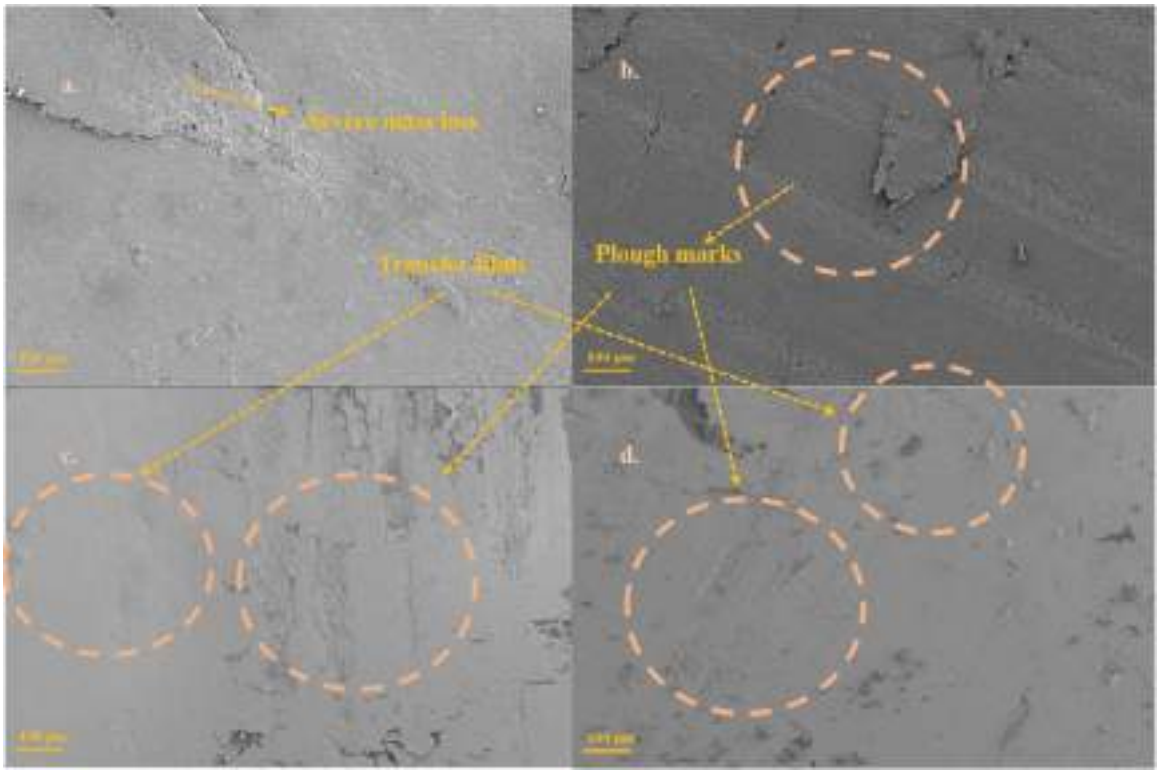

Fig. 13. FESEM images for worn-out surfaces of **a.)** EP, **b.)** ES2, **c.)** EW2, and **d.)** ESW2 at 50 N applied load.

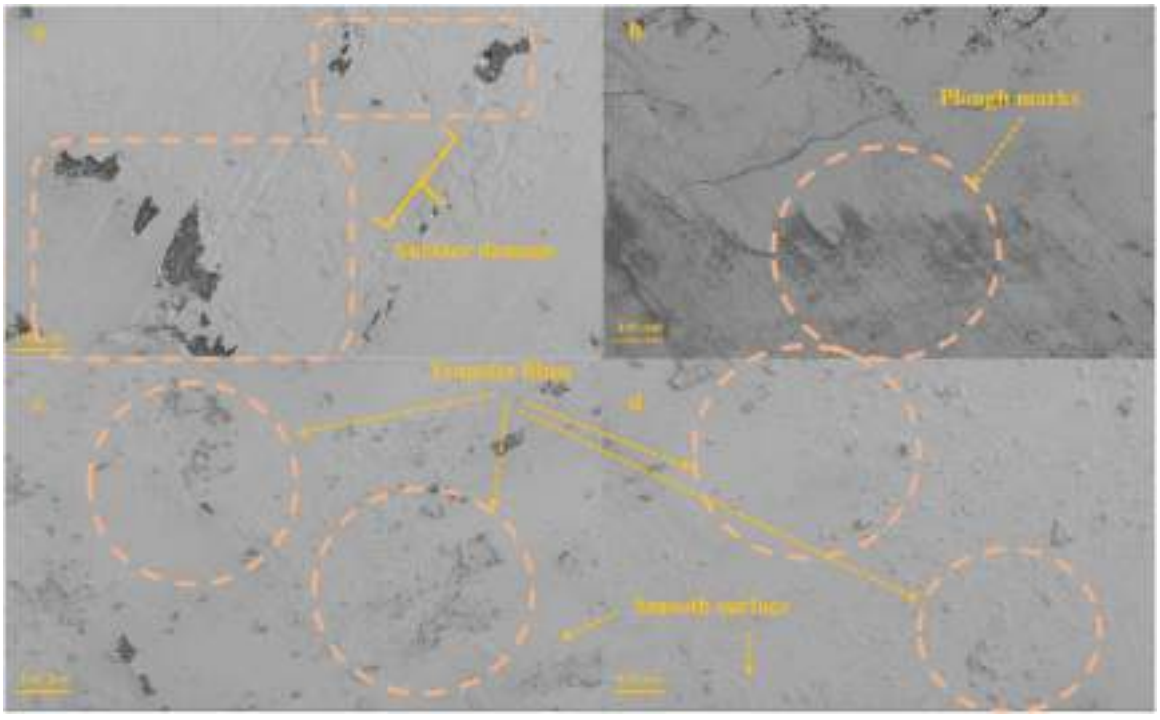

Fig. 14. FESEM images for worn-out surfaces of **a.)** EP, **b.)** ES2, **c.)** EW2, and **d.)** ESW2 at 100 N applied load.

to its very high density, which causes it to experience greater inertial force and normal contact pressure during sliding. As a result, WC are more likely to making them likely to lodge deeply into the transfer film and remain actively engaged at the tribo-interface. Rather than acting abrasively, these hard, spherical WC nanoparticles tend to roll and behave like micro ball bearings, as shown in Fig. 14, promoting fine-scale smoothening of surface asperities. This nano-polishing action significantly contributed to lower COF and enhanced wear resistance, as supported by Fig. 10 **and** Table 6.

3.5.4. Wear and friction modelling

3.5.4.9. Energy wear models. The Fleischer energy model enhances conventional wear prediction approaches by introducing frictional energy density (e_R^*), which quantifies the frictional work per unit volume. Unlike Archard's wear law, which primarily considers contact pressure, Fleischer's model integrates additional parameters such as sliding distance, material properties, temperature rise due to frictional heating, and testing speed. This comprehensive approach makes it especially applicable for evaluating wear in polymeric materials under complex and dynamic conditions. The following models can be calculated using Eq. (9–13) [72].

$$W_R = F_N * S.D * \mu \tag{9}$$

$$V_W = \frac{1}{e_R^*} * W_R \tag{10}$$

$$e_R^* = \frac{1}{K} * \mu * H \tag{11}$$

$$V_W = \frac{\Delta m}{\rho} \tag{12}$$

$$K = \frac{1}{N_c} \tag{13}$$

Where, W_R is the performed frictional work, F_N is the load applied, S. D is the sliding distance, μ is the COF, V_W is the total wear volume, e_R^* is the frictional energy density, K is the wear coefficient, H is the shore D hardness, Δm is the overall mass loss, ρ is the density of the specimen and N_c being the sustainable load cycles. As the filler vol % is very low, the density of the nanocomposites is kept constant to that of neat cured EP, i.e., 1.2 g/cm^3 [73]. The values obtained by using these equations are tabulated in Table 7.

As observed from Table 7, the frictional work (W_R) for EP increases with rising load, which is expected since higher loads generate greater frictional forces, leading to increased energy dissipation at the sliding interface. This trend is evidence of intensified interaction between the specimen and the counterface, resulting in more wear and thermal energy generation. However, the nanocomposites exhibit a slightly different behaviour. For ES2, W_R increases up to 50 N but decreases at 100 N, suggesting improved thermal stability and wear resistance due to enhanced crosslinking. A similar trend is observed in WC-filled nanocomposites (EW2 and ESW2), where W_R initially rises and drops at higher loads. This reduction is attributed to the nanopolishing effect of WC, which helps in maintaining surface integrity and minimize energy loss. These observations highlight the capability of the nanofillers to effectively reduce wear-related energy dissipation under extreme surface contact conditions.

Table 7
Frictional work (W_R), friction energy density (e^*_R), wear coefficient (K) and sustainable number of cycles (Nc) found using the Fleischer energy model for EP, ES2, EW2, and ESW2.

Samples	W_r (kJ)	e^*_r (J/m^3)	K	N_c	
EP	25N	38.96	$2.41 * 10^{12}$	$1.85 * 10^{-11}$	$5.4 * 10^{10}$
	50N	42.73	$2.51 * 10^{11}$	$9.75* 10^{-11}$	$1.02 * 10^{10}$
	100N	45.25	$1.10 * 10^{11}$	$1.17 * 10^{-10}$	$8.5 * 10^{9}$
ES2	25N	45.25	$2.88 * 10^{13}$	$2.17 * 10^{-12}$	$4.6* 10^{11}$
	50N	80.44	$2.29 * 10^{13}$	$2.43 * 10^{-12}$	$4.11 * 10^{11}$
	100N	77.93	$9.74 * 10^{11}$	$2.76 * 10^{-11}$	$3.62 * 10^{10}$
EW2	25N	40.22	$2.31 * 10^{13}$	$2.27 * 10^{-12}$	$4.4 * 10^{11}$
	50N	75.42	$2.67 * 10^{13}$	$1.84* 10^{-12}$	$5.43 * 10^{11}$
	100N	50.28	$6.35 * 10^{11}$	$2.58 * 10^{-11}$	$3.87 * 10^{10}$
ESW2	25N	40.85	$2.47 * 10^{13}$	$2.31 * 10^{-12}$	$4.3 * 10^{11}$
	50N	69.13	$2.76 * 10^{13}$	$1.75* 10^{-12}$	$5.71 * 10^{11}$
	100N	52.79	$1.75 * 10^{12}$	$1.05* 10^{-11}$	$9.52 * 10^{10}$

The decreasing trend in friction energy density (e^*_R) for EP with increasing load is primarily attributed to the thermal softening of the neat matrix. At elevated loads, the substantial frictional heat generated at the sliding interface softens EP, reducing its resistance to shear and lowering energy dissipation per unit volume. While a similar downward trend is observed for the nanocomposites, their frictional energy densities remain significantly higher than EP, indicative of their improved resistance to thermal softening and degradation. At 100 N, ES2, EW2 and ESW2 exhibit energy density increase of 786 %, 477 %, and 1491 %, respectively, with regard to EP. This remarkable enhancement in ESW2 is attributed to the synergistic effects of SiN induced residual curing, which boosts thermal stability and wear resistance, and the nanopolishing behaviour of WC, which maintains surface integrity and minimizes frictional losses.

The wear coefficient (K) for neat EP increased by 427 % when the load increased from 25 N to 50 N, suggestive of more severe material removal under moderate loading conditions, attributed to severe shear and thermal stresses. The decrease observed for 100 N load is likely due to excessive thermal softening of the matrix, leading to smoother sliding with severe mass loss, constantly exposing new polymer layers. ES2 shows a similar trend, with minimal increase from 25 N to 50 N, indicating surface adjustment and microcutting. A drop at 100 N is attributed to the 'hot ball' effect: friction-induced residual curing that enhances crosslinking and hardness, which reduces surface wear. This suggests 50 N is a transitional regime before full thermal stabilization. In contrast, EW2 and ESW2 exhibit a steady decline in K with increasing load, credited to nanopolishing, rolling effect, and transfer film formation of WC nanoparticles, which collectively reduce surface damage and sliding resistance.

The sustainable cycles (N) for EP steadily decrease with increased load, highlighting its poor resistance to thermal softening. In contrast, ES2, EW2 and ESW2 maintain stable N values across all loads, authenticating their enhanced wear resistance and thermal stability. Remarkably, ESW2 demonstrates a clear synergistic effect, indicating efficient stress transfer within the matrix and a combined benefit of the nanofillers' thermal conductivity, resulting in superior load-bearing performance.

3.5.4.10. Influence of surface roughness. The surface roughness values obtained through ImageJ analysis are presented in Fig. 15. At an applied load of 25 N, all nanocomposites exhibited a gradual reduction in surface roughness, demonstrating improved resistance to deformation and material loss. Notably, EW2 showed a decrease of 29 %, attributed to the onset of the nanopolishing effect. This effect is clearly illustrated in Fig. 16, where EP displays numerous pits and a rough surface, while EW2 reveals a significantly smoother morphology.

At 50 N load, only ES2 displayed low surface roughness compared to the other specimens, assigned to its enhanced crosslinking density, which improves surface integrity. In contrast, EW2 and ESW2 showed increases in surface roughness by 56 % and 17 %, respectively. This potential rise is due to incomplete or irregular transfer film formation, as evidenced by the surface profiles in Fig. 17.

At 100 N load, ESW2 displayed the lowest roughness, showing a 78 % reduction, primarily due to the dominant nanopolishing effect imparted by WC nanoparticles. A similar mechanism is observed for

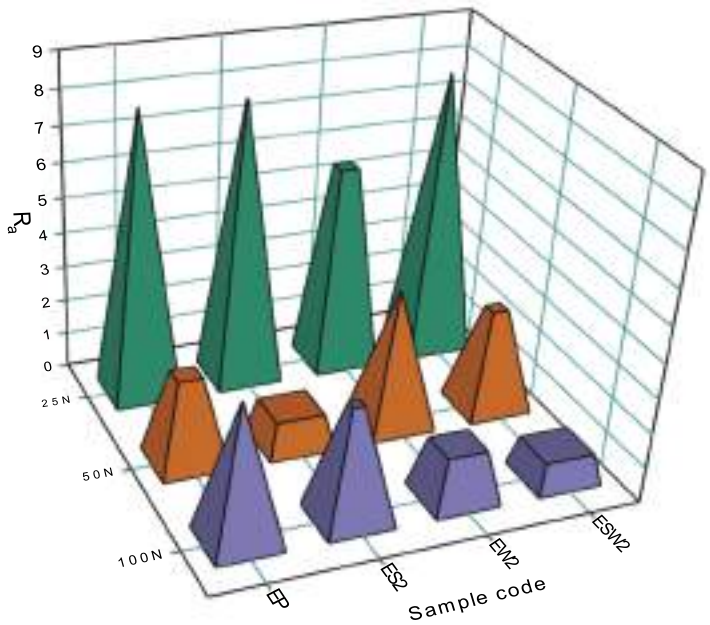

Fig. 15. Surface roughness of EP, ES2, EW2, and ESW2 at 25 N, 50 N, and 100 N.

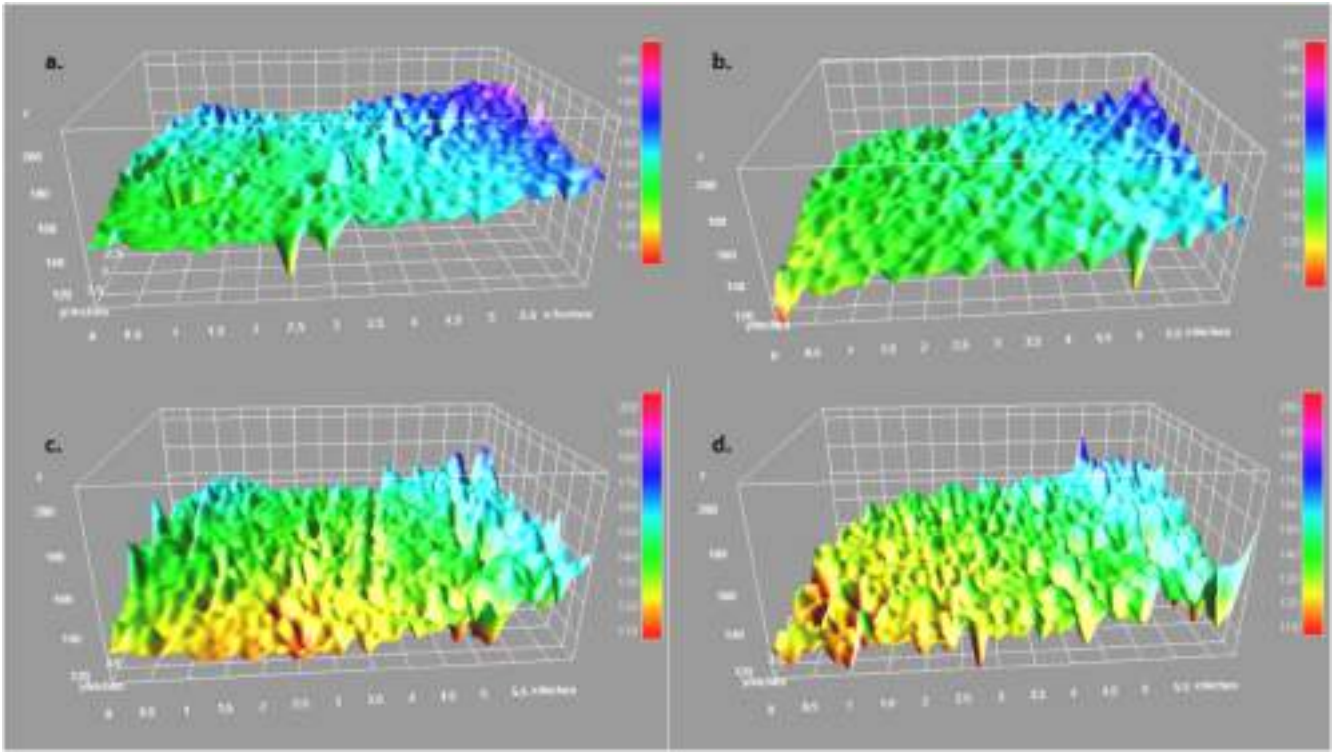

Fig. 16. 3D surface plots of **a.)** EP, **b.)** ES2, **c.)** EW2, and **d.)** ESW2 at 25 N.

EW2, which displayed a 61 % decrease in roughness. In comparison, ES2 showed only a 17 % reduction, due to its increased hardness and micro-ploughing. These mechanisms are evidenced in the surface plots as shown in Fig. 18, where the 3D contour and surface plots highlight the smooth, polished surfaces of EW2 and ESW2, in contrast to the rougher, ploughed texture seen in ES2.

The 3D surface plots, surface roughness measurements, and Fleischer energy-based models collectively confirm that EP undergoes rapid failure due to its poor resistance to thermal softening, degradation, and minimal tolerance to cyclic shear stresses. ES2 demonstrated superior thermal stability, where the nanocomposite maintained structural integrity even under extreme loading conditions, exhibiting a relatively stable surface morphology with an abrasive wear mechanism. However, WC dominated the resistance to wear at higher loads, as observed in EW2 and ESW2, due to the combination of rolling and nanopolishing effects. These mechanisms not only improved the wear resistance but also contributed to a smoother surface finish under dynamic loading conditions. Overall, the synergy between these two nanofillers exponentially enhances the surface properties of EP at very low wt %.

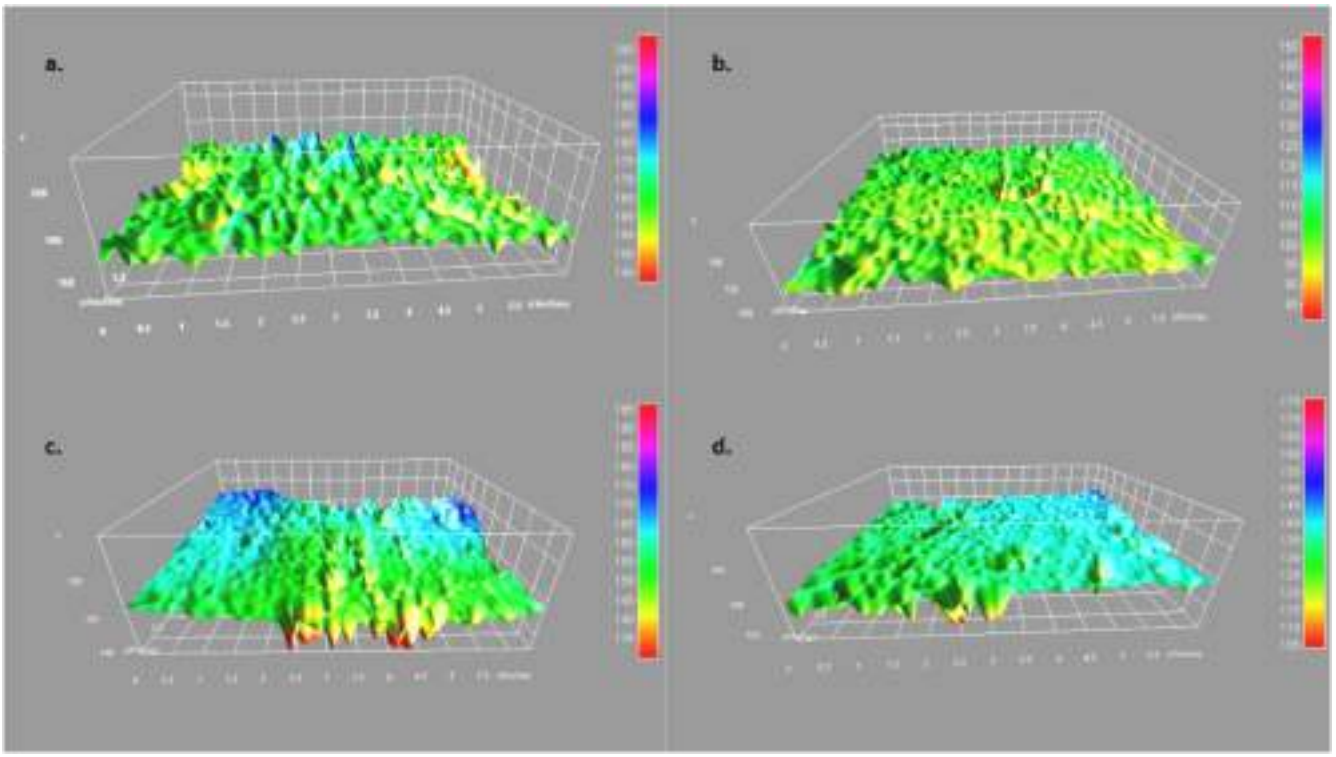

Fig. 17. 3D surface plots of **a.)** EP, **b.)** ES2, **c.)** EW2, and **d.)** ESW2 at 50 N.

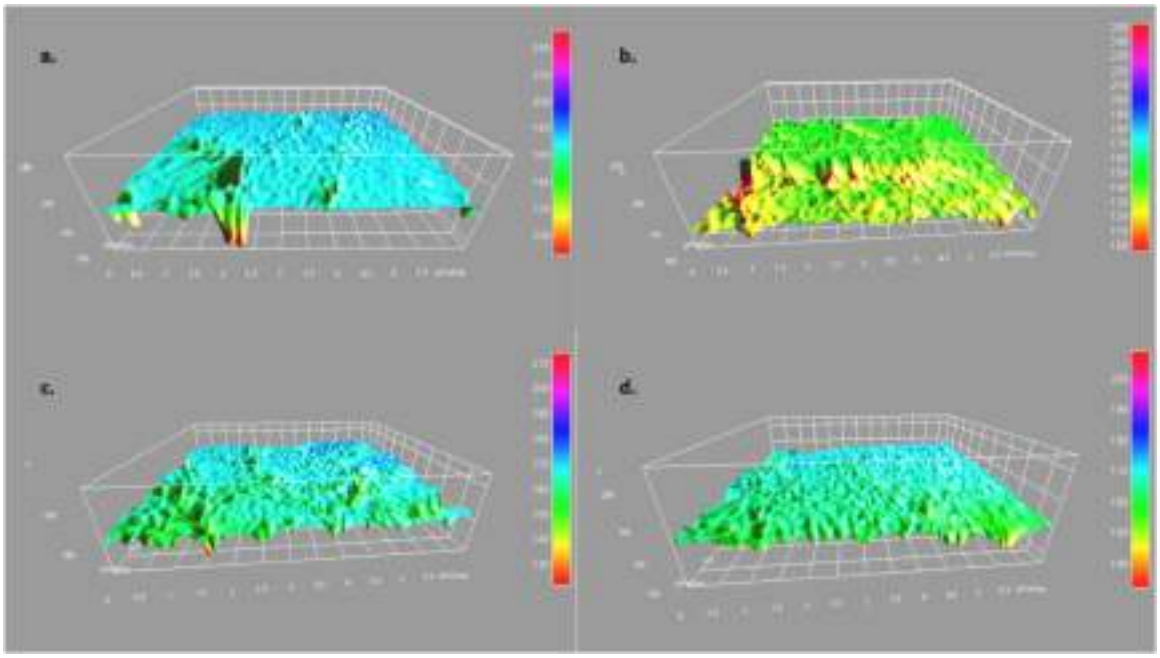

Fig. 18. 3D surface plots of **a.)** EP, **b.)** ES2, **c.)** EW2, and **d.)** ESW2 at 100 N.

3.6. High-Resolution scanning electron microscopy (HR-TEM)

High-resolution transmission electron microscopy (HR-TEM) is one of the most powerful and widely employed characterization tools, providing direct insight into the morphology and dispersion of nano-fillers within a polymer matrix [41]. As shown in Fig. 19, a mutual interaction between SiN and WC is evident, with SiN exhibiting a network-like dispersion with ramified structures [74,75]. These networks create an effective pathway for efficient stress transfer, resulting in enhanced mechanical properties. This interconnected morphology helps in anchoring WC nanoparticles, reducing their agglomeration and promoting a homogenous distribution. Such synergistic arrangements improve filler-filler-matrix interactions, which contributes not only to improved fracture toughness with enhanced energy dissipation, but also to superior wear resistance under abrasive conditions.

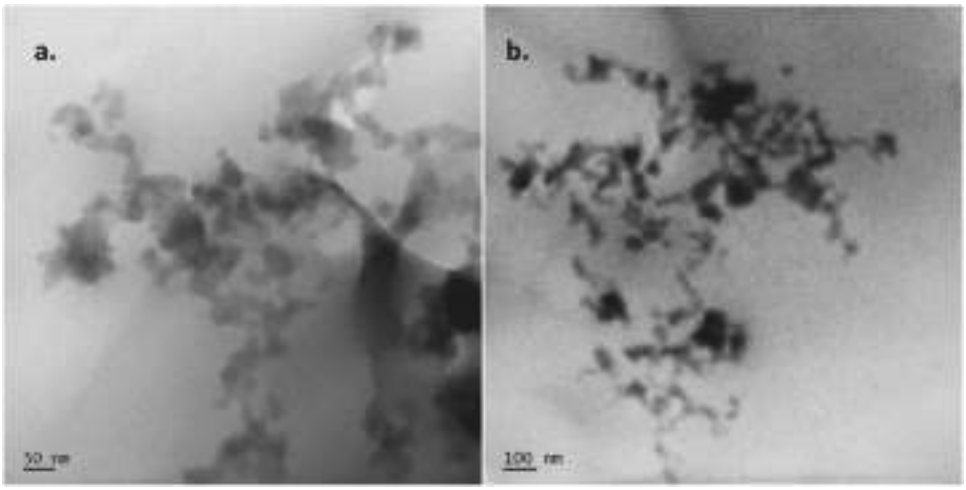

Fig. 19. HR-TEM image of dispersed SiN and WC in ESW2.

4. Conclusion

The study demonstrates that the incorporation of SiN and WC in the EP matrix significantly enhances both mechanical and tribological performance of the nanocomposites. Among the developed hybrid nanocomposites, ESW2 exhibited exceptional performance due to the strong synergistic interaction between the dual nanofillers and the matrix. ESW2 achieved remarkable enhancement in tensile strength, Young's modulus, and strain % by 130 %, 248 %, and 74 %, respectively, compared to neat EP.

The dual nanofillers exhibited distinct toughening and wear mechanisms. SiN enhanced crosslinking density and promoted residual curing or 'hot ball' effect, improving thermal stability and resistance to softening under high loads. WC, on the other hand, imparted a nanopolishing and rolling effect, aided by its high density and inherent hardness, and facilitated the formation of protective transfer films on the wear surface.

Fracture toughness predictions using Irwin's and Huang-Kinloch models aligned well with SiN-based systems but underpredicted the toughness of WC-filled composites. This discrepancy highlights the need to account for additional effects like 'paperweight' and 'anchoring' of WC, which significantly enhance local stress distribution and energy dissipation. Wear behaviour modeled by Fleisher's and modified Archard's approaches, along with surface roughness analysis, further confirmed the nanopolishing and film-forming behaviour of WC, as well as the microcutting and surface hardening effects of SiN. Overall, these dual-filler nanocomposites show immense potential for applications demanding superior wear resistance and mechanical strength under extreme conditions, such as aerospace, automotive, and structural components exposed to abrasive environments.

CRediT authorship contribution statement

Gopal Krishna Bhagavatula: Writing – original draft, Methodology, Investigation, Formal analysis, Data curation, Conceptualization. **Snaha Leena:** Formal analysis, Data curation. **Rasana Nanoth:** Writing – review & editing, Supervision, Formal analysis, Data curation. **Alessandro Pegoretti:** Writing – review & editing. **Jayanarayanan Karingamanna:** Writing – review & editing, Validation, Supervision, Project administration, Methodology, Investigation, Formal analysis, Data curation, Conceptualization.

Declaration of competing interest

The authors declare that they have no known competing financial interests or personal relationships that could have appeared to influence the work reported in this paper.

Acknowledgement

The authors sincerely acknowledge the Department of Mechanical Engineering, Amrita Vishwa Vidyapeetham, Coimbatore, for graciously providing the essential facilities and instrumentation required to carry out the experimental work.

Data availability

Data will be made available on request.

References

[1] Y. Lin, P. Li, W. Liu, J. Chen, X. Liu, P. Jiang, et al., Application-driven high-thermal-conductivity polymer nanocomposites, ACS. Nano 18 (2024) 3851–3870, https://doi.org/10.1021/acsnano.3c08467.

[2] P. Singh, S. Sharma, K. Kumar, S. Lal, G. Iyer, A. Kumar, Synergetic effect of TiO_2 toward mechanically and thermally stable hybrid epoxy nanocomposites: a review, Polym.-Plast. Technol. Mater. 64 (2025) 633–660, https://doi.org/10.1080/25740881.2024.2423365.

[3] W.-D. Hou, F.-L. Guo, D.-Y. Qu, Y.-T. Fu, J.-F. Long, T. Guan, et al., Synergistically improved cryogenic mechanical properties and liquid oxygen compatibility of epoxy nanocomposites by GO and nano-Al(OH)3, Compos. Appl. Sci. Manuf. 192 (2025) 108771, https://doi.org/10.1016/j.compositesa.2025.108771.

[4] W. Chen, Y. Yu, Y. Gu, Y. Ji, J. He, Z. Li, et al., Controllable synthesis of boron nitride submicron tubes and their excellent mechanical property and thermal conductivity applied in the epoxy resin polymer composites, Compos. Appl. Sci Manuf. 154 (2022) 106783, https://doi.org/10.1016/j.compositesa.2021.106783.

[5] W. Chen, J. Yang, B. Li, X. Xu, P. Jin, Z. Wang, New applications of dodecahedral bimetallic imidazolate frameworks in the robust and superior wear-resistant epoxy composites, Front. Chem. Sci. Eng. 19 (2025) 36, https://doi.org/10.1007/s11705-025-2537-2.

[6] W. Chen, J. Yang, F. Zhang, J. Liu, S. Nie, Z. Wang, et al., Significance of structurally inherited nickel/cobalt bimetallic phyllosilicates for enhancing the mechanical, thermal and dry-sliding properties of epoxy composites, Constr. Build. Mater. 472 (2025) 140898, https://doi.org/10.1016/j.conbuildmat.2025.140898.

[7] A. Surnova, D. Balkaev, D. Musin, R. Amirov, A.M. Dimiev, Fully exfoliated graphene oxide accelerates epoxy resin curing, and results in dramatic improvement of the polymer mechanical properties, Compos. B Eng. 162 (2019) 685–691, https://doi.org/10.1016/j.compositesb.2019.01.020.

[8] B. Wetzel, F. Haupert, M. Qiu Zhang, Epoxy nanocomposites with high mechanical and tribological performance, Compos. Sci. Technol. 63 (2003) 2055–2067, https://doi.org/10.1016/S0266-3538(03)00115-5.

[9] S. Srivastava, R.K. Tiwari, Synthesis of epoxy-TiO_2 nanocomposites: a study on sliding wear behavior, thermal and mechanical properties, Int. J. Polym. Mater. 61 (2012) 999–1010, https://doi.org/10.1080/00914037.2011.617326.

[10] M. Padhan, G. Paul, J. Bijwe, Roles of size, shape, amount, and functionalization of nanoparticles of titania in controlling the tribo-performance of UHMWPE composites, Front. Mater. 7 (2020) 205, https://doi.org/10.3389/fmats.2020.00205.

[11] J. Tian, C. Li, G. Xian, Reciprocating friction and wear performances of nanometer SIZED-TiO 2 filled epoxy composites, Polym. Compos. 42 (2021) 2061–2072, https://doi.org/10.1002/pc.25959.

[12] Z. Wang, P. Gu, X. Wu, H. Zhang, Z. Zhang, M.Y.M. Chiang, Micro/nano-wear studies on epoxy/silica nanocomposites, Compos. Sci. Technol. 79 (2013) 49–57, https://doi.org/10.1016/j.compscitech.2013.02.010.

[13] J. Abenojar, J. Tutor, Y. Ballesteros, J.C. Del Real, M.A. Martínez, Erosion-wear, mechanical and thermal properties of silica filled epoxy nanocomposites, Compos. B Eng 120 (2017) 42–53, https://doi.org/10.1016/j.compositesb.2017.03.047.

[14] M.G. Veena, N.M. Renukappa, B. Suresha, K.N. Shivakumar, Tribological and electrical properties of silica-filled epoxy nanocomposites, Polym. Compos. 32 (2011) 2038–2050, https://doi.org/10.1002/pc.21221.

[15] K. Dass, S.R. Chauhan, B. Gaur, Study on the effects of nanoparticulates of SiC, Al 2 O 3, and ZnO on the mechanical and tribological performance of epoxy-based nanocomposites, Part. Sci. Technol. 35 (2017) 589–606, https://doi.org/10.1080/02726351.2016.1184730.

[16] Y. Luo, M. Zhi Rong, M. Qiu Zhang, Tribological behavior of epoxy composites containing reactive SiC nanoparticles, J. Appl. Polym. Sci. 104 (2007) 2608–2619, https://doi.org/10.1002/app.24414.

[17] Q.L. Ji, M.Q. Zhang, M.Z. Rong, B. Wetzel, K. Friedrich, Friction and wear of epoxy composites containing surface modified SiC nanoparticles, Tribol. Lett. 20 (2005) 115–123, https://doi.org/10.1007/s11249-005-8301-3.

[18] G. Shi, M.Q. Zhang, M.Z. Rong, B. Wetzel, K. Friedrich, Friction and wear of low nanometer Si3N4 filled epoxy composites, Wear. 254 (2003) 784–796, https://doi.org/10.1016/S0043-1648(03)00190-X.

[19] M.V. Deepthi, R.R.N. Sailaja, P. Sampathkumaran, S. Seetharamu, S. Vynatheya, High density polyethylene and silane treated silicon nitride nanocomposites using high-density polyethylene functionalized with maleate ester: mechanical, tribological and thermal properties, Mater. Des. 1980-2015 56 (2014) 685–695, https://doi.org/10.1016/j.matdes.2013.11.028.

[20] S. Mandal, P.K. Sain, A. Kabra, N.C. Reger, D. Solanki, R.K. Goyal, et al., Tribological behavior of silicon nitride reinforced polycarbonate nanocomposites, J. Appl. Polym. Sci. 140 (2023) e53807, https://doi.org/10.1002/app.53807.

[21] S. Leena, R. Nanoth, J. Karingamanna, B. SN, S.G.K. Bhagavatula, K.P. Rajan, et al., Investigations on morphology, tribology, rheology, thermo-mechanical properties, and EMI shielding of WC/MWCNT nanohybrids in polypropylene, J. Reinf. Plast. Compos. (2024) 07316844241240565, https://doi.org/10.1177/07316844241240565.

[22] M. Kameswara Reddy, V. Suresh Babu, K.V. Sai Srinadh, M. Bhargav, Mechanical properties of tungsten carbide nanoparticles filled epoxy polymer nano composites, Mater. Today Proc. 26 (2020) 2711–2713, https://doi.org/10.1016/j.matpr.2020.02.569.

[23] D. Athith, M. Sanjay, T. Yashas Gowda, P. Madhu, G. Arpitha, B. Yogesha, et al., Effect of tungsten carbide on mechanical and tribological properties of jute/sisal/E-glass fabrics reinforced natural rubber/epoxy composites, J. Ind. Text. 48 (2018) 713–737, https://doi.org/10.1177/1528083717740765.

[24] V. Verma, H. Tiwari, Role of filler morphology on friction and dry sliding wear behavior of epoxy alumina nanocomposites, Proc. Inst. Mech. Eng. J. J. Eng. Tribol. 235 (2021) 1614–1626, https://doi.org/10.1177/1350650120970433.

[25] Ai N.A., Hussein S.I., Jawad M.K., A. IA. Effect of Al2O3 and SiO2 Nanopartical on Wear, Hardness and Impact behavior of Epoxy composites n.d.

[26] D. Bazrgari, F. Moztarzadeh, A.A. Sabbagh-Alvani, M. Rasoulianboroujeni, M. Tahriri, L. Tayebi, Mechanical properties and tribological performance of epoxy/Al2O3 nanocomposite, Ceram. Int. 44 (2018) 1220–1224, https://doi.org/10.1016/j.ceramint.2017.10.068.

[27] S. Bhatia, S. Khan, S. Angra, Effect of the content of silane-functionalized boron carbide on the mechanical and wear performance of B 4 C reinforced epoxy composites, High Perform. Polym. 33 (2021) 1165–1180, https://doi.org/10.1177/09540083211031129.

[28] J. Yang, X. Feng, S. Nie, Y. Xu, Z. Li, Self-sacrificial templating synthesis of flower-like nickel phyllosilicates and its application as high-performance reinforcements in epoxy nanocomposites, Front. Chem. Sci. Eng. 16 (2022) 484–497, https://doi.org/10.1007/s11705-021-2074-6.

[29] A. Khan, M. Puttegowda, P. Jagadeesh, H.M. Marwani, A.M. Asiri, A. Manikandan, et al., Review on nitride compounds and its polymer composites: a multifunctional material, J. Mater. Res. Technol. 18 (2022) 2175–2193, https://doi.org/10.1016/j.jmrt.2022.03.032.

[30] N. Ramdani, J. Wang, H. Wang, T. Feng, M. Derradji, W. Liu, Mechanical and thermal properties of silicon nitride reinforced polybenzoxazine nanocomposites, Compos. Sci. Technol. 105 (2014) 73–79, https://doi.org/10.1016/j.compscitech.2014.10.006.

[31] X. Cai, H. Wang, Y. Xu, B. Cao, M. Liu, X. Li, Room-temperature wear resistance of tungsten carbide composite layers produced on grey cast iron by diffusion-controlled in situ reactions, Surf. Coat. Technol. 424 (2021) 127649, https://doi.org/10.1016/j.surfcoat.2021.127649.

[32] N. Vidakis, A. Moutsopoulou, M. Petousis, N. Michailidis, C. Charou, V. Papadakis, et al., Rheology and thermomechanical evaluation of additively manufactured acrylonitrile butadiene styrene (ABS) with optimized tungsten carbide (WC) nano-ceramic content, Ceram. Int. 49 (2023) 34742–34756, https://doi.org/10.1016/j.ceramint.2023.08.144.

[33] Z.A.R.A.H. Al Saadi, Z.K. Alobad, M. Akraa, The effect of tungsten carbide nanoparticles on the morphological, mechanical and tribological properties of WC/epoxy and WC/TBCP/epoxy nanocomposite, J. Achiev. Mater. Manuf. Eng. 123 (2024), https://doi.org/10.5604/01.3001.0054.7215.

[34] A. Namdev, A. Telang, R. Purohit, Synthesis and mechanical characterization of epoxy hybrid composites containing graphene nanoplatelets, Proc. Inst. Mech. Eng. C J. Mech. Eng. Sci. 236 (2022) 7984–7998, https://doi.org/10.1177/09544062221081286.

[35] A. Namdev, R. Purohit, A. Telang, Impact of graphene nano particles on tribological behaviour of carbon fibre reinforced composites, Adv. Mater. Process. Technol. 10 (2024) 2809–2826, https://doi.org/10.1080/2374068X.2023.2189670.

[36] B. Satheesan, A.S. Mohammed, Tribological characterization of epoxy hybrid nanocomposite coatings reinforced with graphene oxide and titania, Wear. (2021) 466–467, https://doi.org/10.1016/j.wear.2020.203560, 203560.

[37] S. Gioti, A. Sanida, G.N. Mathioudakis, A.C. Patsidis, T. Speliotis, G.C. Psarras, Multitasking performance of Fe3O4/BaTiO3/epoxy resin hybrid nanocomposites, Materials. (Basel) 15 (2022) 1784, https://doi.org/10.3390/ma15051784.

[38] Y. Song, C. Rong, X. Feng, Y. Liu, Y. Zhang, Heterostructured RGO /MoS2 to improve friction and wear performance of epoxy resins, Polym. Compos. 44 (2023) 8010–8020, https://doi.org/10.1002/pc.27684.

[39] S.G.K. Bhagavatula, S.K. Painkal, R. Nanoth, K. Murugasamy, J. Karingamanna, Synergistic behavior of dual filler system (n -Si 3 N 4 /COOH-MWCNT) on the mechanical, tribological, curing, and corrosion characteristics of epoxy hybrid nanocomposites, J. Appl. Polym. Sci. 140 (2023), https://doi.org/10.1002/app.53778.

[40] C.A. Schneider, W.S. Rasband, K.W. Eliceiri, NIH image to ImageJ: 25 years of image analysis, Nat. Methods 9 (2012) 671–675, https://doi.org/10.1038/nmeth.2089.

[41] G.K. Bhagavatula, S. Leena, K. Murugasamy, R. Nanoth, S. Narayanan, A. Pegoretti, et al., Epoxy nanocomposites with dual filler system: improving surface protection against wear and thermocyclic corrosion, Surf. Interfaces. 55 (2024) 105477, https://doi.org/10.1016/j.surfin.2024.105477.

[42] B. Gopal Krishna, L. Snaha, N. Rasana, K. Jayanarayanan, Effect of nano silicon nitride integration on the curing performance of DGEBA epoxy matrix at ambient temperature, Mater. Lett. 377 (2024) 137410, https://doi.org/10.1016/j.matlet.2024.137410.

[43] Q. Guo, P. Zhu, G. Li, L. Huang, Y. Zhang, D.D. Lu, et al., One-pot synthesis of bimodal silica nanospheres and their effects on the rheological and thermal–mechanical properties of silica–epoxy composites, RSC. Adv. 5 (2015) 50073–50081, https://doi.org/10.1039/C5RA06914A.

[44] L.-C. Tang, H. Zhang, S. Sprenger, L. Ye, Z. Zhang, Fracture mechanisms of epoxy-based ternary composites filled with rigid-soft particles, Compos. Sci. Technol. 72 (2012) 558–565, https://doi.org/10.1016/j.compscitech.2011.12.015.

[45] L. Wenbo, Y. Tingqing, Computer simulation of conic-shaped patterns on fracture surfaces of polymers, J. Appl. Polym. Sci. 89 (2003) 1722–1725, https://doi.org/10.1002/app.12352.

[46] J.-B. Kopp, J. Girardot, Dynamic fracture in a semicrystalline biobased polymer: an analysis of the fracture surface, Int. J. Fract. 226 (2020) 121–132, https://doi.org/10.1007/s10704-020-00482-y.

[47] Linear Elastic Fracture - an overview | ScienceDirect Topics n.d. https://www.sciencedirect.com/topics/materials-science/linear-elastic-fracture (accessed April 19, 2025).

[48] Caddell R.M. Deformation and fracture of solids. No Title 1980.

[49] A.J. Kinloch, D.L. Maxwell, R.J. Young, The fracture of hybrid-particulate composites, J. Mater. Sci. 20 (1985) 4169–4184, https://doi.org/10.1007/BF00552413.

[50] P. Dittanet, R.A. Pearson, Effect of bimodal particle size distributions on the toughening mechanisms in silica nanoparticle filled epoxy resin, Polymer 54 (2013) 1832–1845, https://doi.org/10.1016/j.polymer.2012.12.059.

[51] B.B. Johnsen, A.J. Kinloch, R.D. Mohammed, A.C. Taylor, S. Sprenger, Toughening mechanisms of nanoparticle-modified epoxy polymers, Polymer 48 (2007) 530–541, https://doi.org/10.1016/j.polymer.2006.11.038.

[52] T. Gómez-del Río, A. Salazar, R.A. Pearson, J. Rodríguez, Fracture behaviour of epoxy nanocomposites modified with triblock copolymers and carbon nanotubes, Compos. B Eng. 87 (2016) 343–349, https://doi.org/10.1016/j.compositesb.2015.08.085.

[53] K.T. Faber, A.G. Evans, Crack deflection processes—I. Theory, Acta Metall. 31 (1983) 565–576, https://doi.org/10.1016/0001-6160(83)90046-9.

[54] K.T. Faber, A.G. Evans, Crack deflection processes—II. Experiment, Acta Metall. 31 (1983) 577–584, https://doi.org/10.1016/0001-6160(83)90047-0.

[55] A.J. Kinloch, Fracture Behaviour of Polymers, Springer Science & Business Media, 2013.

[56] K.M. Hamdia, X. Zhuang, P. He, T. Rabczuk, Fracture toughness of polymeric particle nanocomposites: evaluation of models performance using bayesian method, Compos. Sci. Technol. 126 (2016) 122–129, https://doi.org/10.1016/j.compscitech.2016.02.012.

[57] Inernational A. Standard test methods for plane-strain fracture toughness and strain energy release rate of plastic materials. ASTM D5045-99 2007.

[58] Rymuza Z. Tribology of Polymers. Arch Civ Mech Eng 2007;7:177–84. https://doi.org/10.1016/S1644-9665(12)60235-0.

[59] S. Sharma, Tribology of polymeric systems: theory, modeling, and simulation, Tribol. Polym. Polym. Compos. Polym. Nanocompos. (2023) 401–435.

[60] S.C. George, J.T. Haponiuk, S. Thomas, R. Reghunath, P.S. Sarath, Tribology of polymers, Polymer Composites, Polymer Nanocompos. (2022).

[61] Q.J. Wang, Y.-W. Chung, Encyclopedia of Tribology, Springer US, Boston, MA, 2013, https://doi.org/10.1007/978-0-387-92897-5.

[62] A. Dasari, Z.-Z. Yu, Y.-W. Mai, Fundamental aspects and recent progress on wear/scratch damage in polymer nanocomposites, Mater. Sci. Eng. R. Rep. 63 (2009) 31–80, https://doi.org/10.1016/j.mser.2008.10.001.

[63] P. Serles, H. Sun, G. Colas, J. Tam, E. Nicholson, G. Wang, et al., Structure-dependent wear and shear mechanics of nanostructured MoS_2 coatings, Adv. Mater. Interfaces. 7 (2020) 1901870, https://doi.org/10.1002/admi.201901870.
[64] N.L. Clelland, M.P. Pagnotto, R.E. Kerby, R.R. Seghi, Relative wear of flowable and highly filled composite, J. Prosthet. Dent. 93 (2005).
[65] S. Sathees Kumar, K. Kannan, C.H. Nithin Chakravarthy, R. Muthalagu, Wear, friction behaviour and thermal characteristics of tungsten carbide reinforced polyamide composites for gear applications, Mater. Today Proc. 37 (2021) 3352–3358, https://doi.org/10.1016/j.matpr.2020.09.204.
[66] F. Valentini, A. Dorigato, A. Pegoretti, M. Tomasi, G.D. Sorarù, M. Biesuz, Si3N4 nanofelts/paraffin composites as novel thermal energy storage architecture, J. Mater. Sci. 56 (2021) 1537–1550, https://doi.org/10.1007/s10853-020-05247-5.
[67] A. Zambotti, E. Caldesi, M. Pellizzari, F. Valentini, A. Pegoretti, A. Dorigato, et al., Polymer-derived silicon nitride aerogels as shape stabilizers for low and high-temperature thermal energy storage, J. Eur. Ceram. Soc. 41 (2021) 5484–5494, https://doi.org/10.1016/j.jeurceramsoc.2021.04.056.
[68] L. Yin, X. Zhou, J. Yu, H. Wang, C. Ran, Fabrication of a polymer composite with high thermal conductivity based on sintered silicon nitride foam, Compos. Appl. Sci. Manuf. 90 (2016) 626–632, https://doi.org/10.1016/j.compositesa.2016.08.022.
[69] S.G.K. Bhagavatula, S. Leena, R. Nanoth, J. Karingamanna, Novel frictional heat-assisted mechanochemical residual curing of epoxy nanocomposites by silicon nitride nanofiller, Polym. Compos. (2025), https://doi.org/10.1002/pc.29840 pc.29840.
[70] M. Asmael, A. Memarzadeh, A review on recent achievements and challenges in electrochemical machining of tungsten carbide, Arch. Adv. Eng. Sci. 2 (2024) 1–23.
[71] L. Chang, K. Friedrich, Enhancement effect of nanoparticles on the sliding wear of short fiber-reinforced polymer composites: a critical discussion of wear mechanisms, Tribol. Int. 43 (2010) 2355–2364, https://doi.org/10.1016/j.triboint.2010.08.011.
[72] Y.J.J. Jason, H.G. How, Y.H. Teoh, H.G. Chuah, A study on the tribological performance of nanolubricants, Processes 8 (2020) 1372, https://doi.org/10.3390/pr8111372.
[73] J.T. Terwey, M.A. Fourati, F. Pape, G. Poll, Energy-based modelling of adhesive wear in the mixed lubrication regime, Lubricants. 8 (2020) 16.
[74] A. Agrawal, S. Chandraker, S.H.A. Physical, Mechanical and sliding weFar behavior of solid glass microsphere filled epoxy composites, Mater. Today Proc. 29 (2020) 420–426, https://doi.org/10.1016/j.matpr.2020.07.295.
[75] J.C. Sánchez-López, A. Fernández, TEM study of fractal scaling in nanoparticle agglomerates obtained by gas-phase condensation, Acta Mater. 48 (2000) 3761–3771, https://doi.org/10.1016/S1359-6454(00)00174-9.